Meiotic Cellular Rejuvenation is Coupled to Nuclear Remodeling in Budding Yeast

Grant A. King[1, ¶], Jay S. Goodman[1, ¶], Keerthana Chetlapalli[1], Jennifer G. Schick[1], Danielle M. Jorgens[2], Kent L. McDonald[2], and Elçin Ünal[1, §]

[1] Department of Molecular and Cell Biology, University of California, Berkeley, United States, 94720

[2] Electron Microscope Lab, University of California, Berkeley, United States, 94720

[¶] These authors contributed equally to this work

[§] Correspondence: elcin@berkeley.edu

ABSTRACT

Production of healthy gametes in meiosis relies on the quality control and proper distribution of both nuclear and cytoplasmic contents. Meiotic differentiation naturally eliminates age-induced cellular damage by an unknown mechanism. Using time-lapse fluorescence microscopy in budding yeast, we found that nuclear senescence factors – including protein aggregates, extrachromosomal ribosomal DNA circles, and abnormal nucleolar material – are sequestered away from chromosomes during meiosis II and subsequently eliminated. A similar sequestration and elimination process occurs for the core subunits of the nuclear pore complex in both young and old cells. Nuclear envelope remodeling drives the formation of a membranous compartment containing the sequestered material. Importantly, *de novo* generation of plasma membrane is required for the sequestration event, preventing the inheritance of long-lived nucleoporins and senescence factors into the newly formed gametes. Our study uncovers a new mechanism of nuclear quality control and provides insight into its function in meiotic cellular rejuvenation.

INTRODUCTION

Aging occurs as an organism loses its ability to maintain homeostasis over time. The cellular changes that accompany aging have been most extensively characterized in the budding yeast, *Saccharomyces cerevisiae* (Figure 1A; Denoth-Lippuner et al., 2014; Kaeberlein, 2010; Longo et al., 2012). Disrupted protein homeostasis results in the accumulation of carbonylated proteins and protein aggregates that contain oxidatively damaged proteins (Aguilaniu et al., 2003; Erjavec et al., 2007). Many organelles exhibit signs of dysfunction: mitochondria fragment and aggregate, mitochondrial membrane potential decreases, and the vacuole becomes less acidic (Henderson et al., 2014; Hughes and Gottschling, 2012; Veatch et al., 2009). Notably, the nucleus also undergoes a number of changes including enlargement of the nucleolus (Lewinska et al., 2014; Morlot et al., 2018; Sinclair et al., 1997), misorganization of nuclear pore complexes (Lord et al., 2015), and accumulation of extrachromosomal ribosomal DNA (rDNA) circles (Denoth-Lippuner et al., 2014; Sinclair and Guarente, 1997). Many of the cellular changes that accrue with age are conserved across eukaryotes (Colacurcio and Nixon, 2016; David et al., 2010; Sun et al., 2016; Tiku et al., 2017).

In budding yeast mitosis, age-induced damage is asymmetrically retained by the mother cell resulting in the formation of an aged mother cell and a young daughter cell (Mortimer and Johnston, 1959). In contrast, meiotic cells reset aging symmetrically such that all of the meiotic products are born young, independent of their progenitor's age (Unal et al., 2011). Importantly, senescence factors originally present in the aged precursor cells, including protein aggregates, nucleolar damage, and rDNA circles, are

no longer present in the newly formed gametes (Unal and Amon, 2011; Unal et al., 2011). How gametes avoid inheriting age-associated damage and how this event is coupled to the meiotic differentiation program remains unknown.

Meiotic differentiation, also known as gametogenesis, is a tightly regulated developmental program whereby a progenitor cell undergoes two consecutive nuclear divisions, meiosis I and meiosis II, to form haploid gametes. Meiotic differentiation requires extensive cellular remodeling to ensure that gametes inherit the necessary nuclear and cytoplasmic contents. In yeast gametogenesis, the nucleus undergoes a closed division, with the nuclear envelope remaining continuous until karyokinesis forms four new nuclei (Moens, 1971; Moens and Rapport, 1971; Neiman, 2011). Mitochondria and cortical endoplasmic reticulum also undergo regulated morphological changes, separating from the cellular cortex and localizing near the nuclear envelope at the transition between meiosis I and II (Gorsich and Shaw, 2004; Miyakawa et al., 1984; Sawyer et al., 2019; Stevens, 1981; Suda et al., 2007). Around the same time, new plasma membranes, also known as prospore membranes, grow from the centrosome-equivalent spindle pole bodies embedded in the nuclear envelope. This directed growth of plasma membrane ensures that nascent nuclei and a fraction of the cytoplasmic contents are encapsulated to form gametes (Brewer et al., 1980; Byers, 1981; Knop and Strasser, 2000; Moens, 1971; Neiman, 1998). Subsequently, the uninherited cellular contents are destroyed by proteases released upon permeabilization of the progenitor cell's vacuole, the yeast equivalent of the mammalian lysosome (Eastwood et al., 2012;

Eastwood and Meneghini, 2015). Whether these cellular remodeling events are integral to the removal of age-induced damage has not been characterized.

In this study, we aimed to determine the mechanism by which nuclear senescence factors are eliminated during budding yeast meiosis. Using time-lapse fluorescence microscopy, we found that protein aggregates, rDNA circles, and a subset of nucleolar proteins are sequestered away from chromosomes during meiosis II. Importantly, we show that the core subunits of the nuclear pore complex (NPC) also undergo a similar sequestration process in both young and old cells. The damaged material localizes to a nuclear envelope-bound compartment containing the excluded NPCs that is eliminated upon vacuolar lysis. Finally, we found that the proper development of plasma membranes is required for the sequestration of core NPCs and senescence factors away from the newly forming gametes. Our study defines a key nuclear remodeling event and demonstrates its involvement in the elimination of age-induced cellular damage during meiotic differentiation.

RESULTS

Senescence factors are sequestered away from chromosomes in meiosis II and subsequently eliminated

To gain a deeper understanding of gametogenesis-induced rejuvenation, we first sought to characterize the meiotic dynamics of age-induced protein aggregates, rDNA circles, and other nucleolar damage using time-lapse fluorescence microscopy. All three types

of damage have been reported to localize to the nuclear periphery in old mitotic cells (Figure 1A; Cabrera et al., 2017; Denoth-Lippuner et al., 2014; Saarikangas et al., 2017; Sinclair and Guarente, 1997). Therefore, we monitored their meiotic localization relative to chromosomes, marked with a fluorescently tagged chromatin protein: either histone H2A (Hta1) or histone H2B (Htb1).

Similar to mitosis, we observed that protein aggregates, visualized by the fluorescently tagged chaperone Hsp104-GFP (Glover and Lindquist, 1998; Saarikangas et al., 2017), localized to a perinuclear region inside the nucleus prior to the meiotic divisions and in meiosis I (Figure 1B, right panel; Figure 1 – Figure Supplement 1). In contrast, during meiosis II, the protein aggregates localized away from chromosomes, a phenomenon we termed sequestration (Figure 1B, 1D; video 1). The sequestration was highly penetrant (>99%) and occurred with consistent timing shortly after the onset of anaphase II (Figure 1D). Subsequently, the aggregates disappeared late in gametogenesis (Figure 1B, right panel; video 1). By comparison, young cells did not contain any Hsp104-associated aggregates but instead displayed diffuse Hsp104 signal throughout meiosis (Figure 1B, left panel). We conclude that age-associated protein aggregates undergo stereotypical sequestration and elimination during meiotic differentiation, suggesting developmentally controlled induction of these events.

We next tested whether the extrachromosomal rDNA circles that accumulate in aged cells displayed a similar behavior. To visualize ribosomal DNA in single cells, we used a strain carrying five tandem copies of the tetracycline operator sequence integrated

within each rDNA repeat in one of the two chromosome XII homologs (tetO-rDNA). The strain additionally contained a tetracycline repressor protein fused to GFP (TetR-GFP) under the control of a meiotic promoter (Li et al., 2011). These two modifications, namely the meiosis-restricted expression of TetR-GFP and the heterozygosity of the tetO-rDNA array, did not affect growth rate in vegetative cells. Using this method, we observed that, in old cells, a substantial fraction of the tetO-rDNA/TetR-GFP signal and a small fraction of the Hta1-mApple signal were sequestered away from chromosomes after the onset of anaphase II and disappeared during late stages of gamete maturation (Figure 1C, right panel; Figure 1E; video 2). By comparison, in young cells, the gamete nuclei retained the entire tetO-rDNA array and histone-bound chromatin after completion of anaphase II (Figure 1C, left panel), consistent with previous work (Fuchs and Loidl, 2004; Li et al., 2011). In aged cells carrying TetR-GFP without the tetO-rDNA array, the GFP signal remained diffuse throughout meiosis (Figure 1 – Figure Supplement 2), confirming that the extrachromosomal GFP puncta were due to sequestered rDNA circles as opposed to TetR-GFP aggregation. These findings demonstrate that, similar to age-associated protein aggregates, extrachromosomal rDNA circles also undergo programmed sequestration and destruction during meiotic differentiation.

In addition to rDNA circles, other nucleolar aberrations also accumulate during cellular aging. As a mother cell continues to divide mitotically, factors involved in ribosomal biogenesis are upregulated, leading to the formation of enlarged and fragmented nucleoli (Janssens et al., 2015; Morlot et al., 2018; Sinclair et al., 1997). To visualize

nucleoli in more detail, we fluorescently tagged the rRNA processing factor Nsr1 at its endogenous locus (Lee et al., 1992). A previous study found that two other rRNA processing factors, the fibrillarin homolog Nop1 and the high mobility group protein Nhp2, are partially sequestered away from chromosomes during gametogenesis (Fuchs and Loidl, 2004). Nsr1 similarly demonstrated partial sequestration after the onset of anaphase II in young cells (Figure 2A). In aged cells, Nsr1 foci appeared enlarged and fragmented prior to the meiotic divisions, consistent with previously reported changes in nucleolar morphology (Figure 2B; Janssens et al., 2015; Morlot et al., 2018; Sinclair et al., 1997). As in young cells, Nsr1 was sequestered away from chromosomes following the onset of anaphase II and subsequently eliminated (Figure 2B-C; video 3). Interestingly, a significantly higher fraction of the total Nsr1 was sequestered in older cells (mean = 23% for 0-3 generation-old cells, 36% for 5-8 generation-old cells and 42% for 9 or more generation-old cells; Figure 2D). A portion of the histone H2B (Htb1-mCherry) was also sequestered away from the gamete nuclei, reminiscent of the behavior of histone H2A in the GFP-marked rDNA strain. This chromatin demarcation occurred only in aged cells and always co-localized with the sequestered nucleoli. Since the extrachromosomal histone mass is present in aged cells independent of the GFP-marked rDNA array, the discarded rDNA circles are likely assembled into chromatin, and the extrachromosomal histone signal can be used as a proxy for rDNA circles.

Finally, we analyzed the behavior of protein aggregates with respect to nucleoli and found that both the timing and location of the sequestration event were coincident (Figure 2E-F). Taken together, these data reveal that distinct types of age-induced

damage all undergo a spatiotemporally linked sequestration and elimination process, suggesting a common mode of meiotic regulation.

Core nucleoporins exhibit a meiotic behavior similar to senescence factors

Since nucleolar constituents localize away from dividing chromosomes even in young cells, we reasoned that the sequestration of age-induced nuclear damage might involve a nuclear remodeling event that generally takes place as part of meiotic differentiation. As a means of assessing nuclear behavior, we sought to characterize the dynamics of nuclear pore complexes during meiosis.

Nuclear pore complexes (NPCs) are large protein structures that span the nuclear envelope and primarily function in selective nucleocytoplasmic transport. NPCs contain multiple copies of at least 30 distinct types of proteins termed nucleoporins. Nucleoporins are organized into six different sub-complexes with distinct structural roles (Beck and Hurt, 2017). Intriguingly, one nucleoporin, Nsp1, has been previously shown to localize away from chromosomes in meiosis II (Fuchs and Loidl, 2004). Using time-lapse microscopy, we surveyed the meiotic dynamics and localization of 17 different endogenously GFP-tagged nucleoporins, representing each NPC subcomplex (Figure 3A). We found that nucleoporins from five of the six subcomplexes, including those most integral to the NPC structure, exhibited sequestration and elimination similar to age-induced damage. The nucleoporins localized to the nuclear periphery before the meiotic divisions and during meiosis I, but largely localized away from chromosomes after the onset of anaphase II (Figure 3B-F; Figure 3 – Supplement 1-5; video 4).

Several hours after the meiotic divisions, any remaining nucleoporin signal abruptly disappeared (Figure 3A-F; Figure 3 – Supplement 1-5; video 4)

Interestingly, the nucleoporins from one subcomplex, the nuclear basket, exhibited a markedly different behavior: although briefly localizing outside of the developing nuclei during anaphase II along with the nucleoporins from other subcomplexes, they returned to the nascent nuclei within 30 minutes (Figure 3G-H; Figure 3 – Supplement 6; video 5). The simplest interpretation of these findings was that the nuclear basket detached from the rest of the NPC during meiosis II. Given that all other NPC subcomplexes persist outside of developing nuclei, we propose that intact NPCs without nuclear baskets are left outside of gamete nuclei.

Since senescence factors and NPCs were sequestered with similar timing, we next asked whether they were sequestered to a similar location. We monitored the localization of protein aggregates, rDNA circles, and sequestered nucleolar material relative to NPCs and found that they co-localize with the sequestered NPCs after the onset of anaphase II (Figure 4A-C; Figure 4 – Supplement 1-2). These results suggest that a common nuclear remodeling event is responsible for the spatial separation of various nuclear components from the dividing chromosomes.

Sequestered nuclear material localizes to a nuclear envelope-bound compartment

The nuclear envelope remains continuous during budding yeast meiosis, dynamically changing shape to accommodate the chromosomal divisions (Moens, 1971; Moens and

Rapport, 1971). After the second meiotic division, karyokinesis occurs to form the nascent nuclei of the four gametes. Given the abrupt change in NPC distribution during anaphase II, we sought to determine how other nuclear membrane proteins behave during this time. We found that the integral LEM-domain protein Heh1 and a generic inner nuclear membrane marker, eGFP-h2NLS-L-TM, localized to both nascent gamete nuclei and the sequestered NPCs during anaphase II (Figure 5A-B; Figure 5 – Supplement 1; King et al., 2006; Meinema et al., 2011), suggesting the existence of a separate membranous compartment.

We next performed serial section transmission electron microscopy (TEM) to observe this compartment directly. Reconstructions of individual cells, either during anaphase II or during gamete development, confirmed the existence of nuclear envelope-bound space outside of the four nuclei (Figure 5C-D; videos 6-9). The compartment appeared deformed in comparison to the nascent gamete nuclei in that the nuclear envelope membrane structure appeared abnormal and the compartment was often fragmented into multiple nuclear envelope-bound regions (Figure 5C-5F; videos 6-9). These regions were located outside of the gamete plasma membranes, also known as prospore membranes (Figure 5C-D; videos 6-9). Importantly, individual sections showed that the compartment contained nucleolar material and NPCs (Figure 5E and 5F; Figure 5 – Supplement 2; videos 6 and 8). We conclude that, during meiosis II, the nuclear envelope undergoes a five-way division to form the four nuclei and a separate compartment containing discarded nuclear proteins.

Core nucleoporins and senescence factors are excluded from developing gametes during meiosis II

The TEM analyses showed that the nuclear envelope-bound compartment localized outside of the developing gamete plasma membranes (Figure 5C-D; videos 6-9). It remained unclear, however, how the material was sequestered into this compartment. At least two models could explain how the material was left outside of the nascent gametes: (1) the material was being "extruded," removed from the gamete after initial entry, or (2) "excluded," never entering the nascent gametes. To differentiate between these models, we analyzed the localization of a gamete-specific plasma membrane (PM) marker, GFP-Spo20$^{51-91}$ (Nakanishi et al., 2004), relative to NPCs and chromosomes. We found that, throughout anaphase II, a sequestered mass of nucleoporins was constrained to a region immediately outside of the nascent plasma membranes and never appeared inside (Figure 6A). The lip of the developing plasma membranes marked by Don1-GFP neatly delineated the boundary of the NPC mass (Figure 6B). Live-cell microscopy confirmed that the NPCs remained outside of nascent plasma membranes throughout their development, supporting "exclusion" as the means by which nuclear material remained outside of the developing gametes (Figure 6 – Supplement 1-2).

To determine if senescence factors were similarly excluded, we monitored the localization of protein aggregates and nucleolar material relative to the gamete plasma membranes. This analysis revealed that age-induced damage almost never entered into newly forming gametes (Figure 6C; Figure 6 – Supplement 3; video 10). Only one out of

several hundred gametes inherited the Hsp104-associated protein aggregates (Figure 6D, Figure 6 – Supplement 3; video 11); strikingly, this Hsp104 punctum persisted after gamete maturation, suggesting that the elimination of age-associated damage is dependent on its prior exclusion. These results highlight the existence of an active mechanism in meiotic cells that precludes the inheritance of NPCs and senescence factors by the nascent nuclei.

Elimination of excluded nuclear material coincides with vacuolar lysis

Following gamete formation, permeabilization of the precursor cell's vacuolar membrane causes the release of proteases, which degrade the cellular contents left in the precursor cell cytosol in a process termed mega-autophagy (Eastwood et al., 2012; Eastwood and Meneghini, 2015). To determine whether mega-autophagy was responsible for the degradation of the excluded nuclear material, we monitored the disappearance of NPCs and age-associated protein aggregates relative to the lysis of the vacuolar membrane as monitored by Vph1-GFP. We found that both events coincided with the onset of vacuolar lysis (Figure 7A-D; videos 12-13). To further assess nucleoporin degradation, we measured the protein levels of GFP-tagged Nup84 and Nup170 by immunoblotting (Figure 7E-F). Since GFP is relatively resistant to vacuolar proteases, degradation of tagged proteins leads to the accumulation of free GFP (Kanki and Klionsky, 2008). We found that free GFP accumulated in wild-type cells 12 hours after meiosis induction, consistent with vacuolar proteases driving the elimination of Nup84 and Nup170 (Figure 7E-F). Importantly, we confirmed that the degradation of both nucleoporins depends on the meiotic transcription factor Ndt80. Ndt80 is a master

transcription factor necessary for the meiotic divisions and gamete maturation (Xu et al., 1995). In the absence of *NDT80*, cells exhibit a prolonged arrest during prophase I and fail to undergo vacuolar lysis (Eastwood et al., 2012). Altogether, these analyses highlight mega-autophagy as the probable degradation mechanism for NPCs and nuclear senescence factors.

Sequestration of nuclear pore complexes requires gamete plasma membrane development

What drives the nuclear remodeling event in meiotic cells? Given that the boundaries of the excluded NPC mass co-localize with the lips of developing gamete plasma membranes (Figure 6B), we hypothesized that plasma membrane development itself might be required for NPC sequestration. To test this hypothesis, we monitored NPC localization in mutants with disrupted plasma membrane formation. Plasma membrane development is initiated from the cytoplasmic face of the spindle pole body, which is converted from a microtubule-nucleation center to a membrane-nucleation center during meiosis II (Knop and Strasser, 2000). *SPO21* (also known as *MPC70*) is required for this conversion event, and its deletion completely inhibits *de novo* plasma membrane formation (Knop and Strasser, 2000). We found that, in *spo21Δ* cells, nucleoporins remained around chromosomes during anaphase II instead of being sequestered away (Figure 8A-B; video 14).

As an independent test of the role of plasma membrane development in NPC remodeling, we perturbed plasma membrane development by an orthogonal method.

The formation of fewer than four plasma membranes can be induced by low carbon conditions, since carbon concentration affects the conversion of the spindle pole body into a membrane nucleator (Davidow et al., 1980; Okamoto and Iino, 1981; Taxis et al., 2005). Under such conditions, we found that the gamete nuclei displayed reciprocal localization of plasma membranes and NPCs: only the nuclei that were devoid of plasma membranes were enriched for NPCs (Figure 8C-E). This was consistent with the observation that, even in high carbon conditions, cells fated to form three or two mature gametes would often have one or two nuclei enriched for NPCs, respectively (Figure 8B).

Finally, we examined how defects in leading edge complex formation, the structure that forms at the lip of the developing plasma membranes, affect NPC sequestration. Specifically, the absence of the organizing member Ssp1 or simultaneous deletion of the Ady3 and Irc10 subunits, results in the formation of misshapen plasma membranes (Lam et al., 2014; Moreno-Borchart et al., 2001). We found that both *ssp1Δ* and *ady3Δ irc10Δ* cells had defective NPC sequestration, with NPCs often remaining partially around anaphase II nuclei (Figure 8F; Figure 8 – Supplement 1-2). The boundary of NPC removal from the nuclei was marked by constrictions in the DAPI signal and corresponded to the extent of plasma membrane formation (Figure 8F; Figure 8 – Supplement 1-2). Taken together, these data support the conclusion that NPC sequestration and exclusion are driven by the development of plasma membranes around nascent gamete nuclei.

Sequestration of senescence factors requires proper plasma membrane development

Since the sequestration of NPCs and nuclear senescence factors were spatially and temporally coupled, we reasoned that a common mechanism could mediate both events. We therefore monitored the sequestration of protein aggregates in *spo21Δ* cells, which are defective in NPC sequestration. In comparison to wild-type cells, we found that *spo21Δ* mutants exhibited a dramatic increase in the association of protein aggregates with chromosomes during anaphase II (52% vs. 0%; Figure 9A-B). Regardless of whether or not the protein aggregate was sequestered away from chromosomes in *spo21*Δ cells, the protein aggregates always co-localized with the nuclear envelope, as marked by NPCs (Figure 9 – Supplement 1). Thus, without the nascent plasma membranes, protein aggregates appeared randomly distributed along the nuclear periphery.

We next assessed how nucleolar sequestration is affected in *spo21Δ* cells by monitoring the formation of the sequestered Nsr1 focus. We found that in 39% of the *spo21Δ* cells, the nucleoli failed to be sequestered in meiosis II and instead co-segregated with chromosomes. In contrast, none of the wild-type cells displayed this behavior (Figure 9C-D). Furthermore, Nsr1 remained co-localized to the nuclear envelope in *spo21Δ* cells in a similar manner to protein aggregates (Figure 9 – Supplement 2). Altogether, these findings support the notion that meiotic exclusion of age-induced protein aggregates and nucleolar material is coupled to a nuclear remodeling event that is driven by gamete plasma membrane formation.

DISCUSSION

This study defines a meiotic quality control mechanism that eliminates nuclear senescence factors in budding yeast. In an aged precursor cell, many of its nuclear contents, including nuclear pore complexes, rDNA circles, nucleolar proteins and protein aggregates, are sequestered in a membranous compartment away from the chromosomes that are destined for future gametes (Figure 10). The discarded compartment and its contents are eliminated upon programmed lysis of the vacuole, an organelle functionally equivalent to the lysosome. We further show that *de novo* plasma membrane growth is required for the sequestration of nuclear material (Figure 10). Together, our findings define a meiosis-specific nuclear remodeling event that physically separates age-induced cellular damage away from gametes and highlights its role in cellular rejuvenation.

Selective inheritance of nuclear contents during meiotic differentiation

We found that a subset of nuclear components are sequestered away from chromosomes during anaphase II: core nucleoporins, nucleolar proteins involved in rRNA transcription and processing, extrachromosomal rDNA circles, and protein aggregates. However, other nuclear proteins – including histones, the rDNA-associated protein Cfi1, and the Ran exchange factor Prp20 – are largely retained with dividing nuclei during anaphase II (unpublished data). A more thorough cataloging of nuclear components is needed to identify parameters that differentiate excluded nuclear material from retained nuclear material. Strong association with chromatin, as in the

case for histones, Cfi1 and Prp20, may be one way to mediate the selective inheritance of nuclear proteins into gametes. On the other hand, strong association with NPCs may facilitate sequestration – for example, extrachromosomal rDNA circles have been shown to interact with NPCs in mitotic cells (Denoth-Lippuner et al., 2014).

Unexpectedly, we found that nuclear basket nucleoporins dissociate from the rest of the nuclear pore complex and remain with nascent nuclei during meiosis II. In both vertebrates and in the fungus *Asperilligus nidulans*, the nuclear basket nucleoporin Nup2 and its metazoan ortholog Nup50 associate with dividing chromatin during mitosis and contribute to the segregation of NPCs into daughter nuclei (Dultz et al., 2008; Markossian et al., 2015; Suresh et al., 2017). We propose that the nuclear basket segregates with gamete nuclei through re-association with chromatin, which in turn facilitates the formation of new NPCs. The nuclear basket nucleoporins Nup1 and Nup60 have innate membrane binding and shaping capabilities, making them attractive candidates to initiate insertion of new NPCs (Meszaros et al., 2015). Indeed, deletion of non-essential nuclear basket nucleoporins results in reduced sporulation efficiency and impaired gamete viability, supporting an important functional role during the meiotic program (Chu and Burgess, 2016)

Formation of gamete plasma membranes is required for the sequestration of nuclear material

We found that gamete plasma membrane formation is required for the selective sequestration of nuclear contents. When plasma membrane development is prevented,

NPCs are retained and age-induced damage becomes randomly distributed along the nuclear periphery. The mechanism by which the newly forming plasma membrane creates distinct nuclear envelope domains inside and outside of developing gametes remains unclear. A direct physical blockade, while possible, seems unlikely given that large organelles such as mitochondria enter through the lips of developing plasma membranes (Byers, 1981; Suda et al., 2007). On the other hand, the sequestration boundary at the leading edge is reminiscent of the outer nuclear envelope lateral diffusion barrier that forms at the bud neck during budding yeast mitosis (Caudron and Barral, 2009; Clay et al., 2014). In this context, septins localize to the bud neck and organize a signaling cascade, generating a sphingolipid region in the nuclear envelope that constrains the movement of nuclear envelope proteins (Clay et al., 2014). In meiosis, deletion of meiosis-specific septins (*spr3Δ* and *spr28Δ*; De Virgilio et al., 1996; Fares et al., 1996; Ozsarac et al., 1995) and leading edge complex components (*ady3Δ*, *irc10Δ*, and *don1Δ*; Knop and Strasser, 2000; Lam et al., 2014; Moreno-Borchart et al., 2001) does not grossly alter NPC or protein aggregate sequestration, beyond impacting plasma membrane morphology (Figure 8F; Table S5). However, an unidentified scaffold might exist to organize a nuclear envelope diffusion barrier. Determining the mechanism by which gamete plasma membranes sequester nuclear material will reveal important principles of nuclear organization and compartmentalization.

A five-way nuclear division facilitates the subsequent elimination of discarded nuclear material by vacuolar lysis

The sequestration of nuclear damage into a membranous compartment outside of gametes makes it accessible to the degradation machinery active in the progenitor cell cytoplasm during gamete maturation. Due to the strong correlation between the timing of vacuolar lysis and the disappearance of sequestered material as well as the meiosis-specific appearance of NPC degradation intermediates, we propose that mega-autophagy is responsible for the elimination of nuclear senescence factors (Eastwood et al., 2012; Eastwood and Meneghini, 2015). Consistent with this, vacuolar protease levels are upregulated during gamete maturation, while other factors involved in canonical protein degradation pathways, including the ubiquitin proteasome system and macroautophagy, are downregulated (Brar et al., 2012; Cheng et al., 2018; Eisenberg et al., 2018). The release of vacuolar proteases from the vacuole could eliminate protein aggregates and other sequestered nuclear proteins, as has already been observed for unsuccessfully packaged nuclei (Eastwood et al., 2012). Another mechanism, however, is necessary for the elimination of rDNA circles. The endonuclease G homolog, Nuc1, is released from mitochondria during mega-autophagy, could be responsible for the elimination of rDNA circles (Eastwood et al., 2012).

Nuclear remodeling as a driver of gamete health and rejuvenation

Our study highlights a mechanism that facilitates the elimination of age-induced damage during meiosis. Given that extensive nuclear remodeling occurs even in young cells, the reorganization of the nuclear periphery appears to be integral to gamete fitness. Importantly, the sequestration of NPCs in budding yeast meiosis is similar to a NPC reorganization event observed in the spermatogenesis of metazoans, including humans

(Fawcett and Chemes, 1979; Ho, 2010; Troyer and Schwager, 1982). In this context, acrosome formation, potentially akin to gamete plasma membrane formation, corresponds to the redistribution of nuclear pores to the caudal end of the nucleus, facilitating chromatin condensation and elimination of un-inherited nuclear material. Whether removal of age-induced damage is also coupled to nuclear remodeling during metazoan spermatogenesis remains to be determined.

Elimination of age-induced damage during gamete maturation may be integral to gamete rejuvenation. In *C. elegans* gametogenesis, oocyte maturation involves the elimination of age-induced protein aggregates by lysosomal activation (Bohnert and Kenyon, 2017; Goudeau and Aguilaniu, 2010). Further determining the mechanism of age-induced damage sequestration and elimination could aid in the development of strategies to counteract cellular aging in somatic cells. The selective inheritance of distinct types of age-induced damage could provide a means of determining whether a given senescence factor is a cause or consequence of aging. In this manner, meiotic differentiation offers a unique and natural context to uncover quality control mechanisms that eliminate the determinants of cellular aging.

MATERIALS AND METHODS

Yeast strains, plasmids and primers

All strains in this study are derivatives of SK1 and specified in Table S1. Strains UB17338, UB17509 and UB17532 are derivatives of strain HY2545 (a gift from Dr.

Hong-Guo Yu). Deletion and C-terminal tagging at endogenous loci were performed using previously described PCR-based methods unless otherwise specified (Janke et al., 2004; Longtine et al., 1998; Sheff and Thorn, 2004). Deletion of *SSP1* was performed by transforming cells with a PCR amplicon of the locus from the SK1 yeast deletion collection (a gift from Dr. Lars Steinmetz). Primer sequences for strain construction are specified in Table S2. The following strains were constructed in a previous paper: *flo8Δ* (Boselli et al., 2009), the *pGAL-NDT80 GAL4-ER* system (Carlile and Amon, 2008), Htb1-mCherry (Matos et al., 2008), Hsp104-GFP (Unal et al., 2011), *ndt80Δ* (Hochwagen et al., 2005), and *spo21Δ* (Sawyer et al., 2019).

To visualize the vacuole, we used either an eGFP-tagged version of Vph1 integrated at the *HIS3* locus or a mCherry-tagged version of Vph1 at its endogenous locus. To generate the eGFP-tagged version, we amplified the SK1 genomic region from 1000 bp upstream to immediately before the stop codon of *VPH1* (2520 bp after the ORF start) and fused it to yeGFP in the *HIS3* integrating plasmid pLC603 (a gift from Leon Chan). We then performed integration at the *HIS3* locus by cutting the plasmid with PmeI. To generate the mCherry-tagged version, we constructed a new *HIS3*-selectable mCherry plasmid by replacing eGFP in pYM28 (Janke et al., 2004) with mCherry. We then tagged the locus via traditional PCR-based methods.

To visualize the nuclear envelope, we generated an inner nuclear membrane-localizing reporter (eGFP-h2NLS-L-TM) by fusing eGFP and amino acids 93 to 378 of Heh2 (Meinema et al., 2011) under control of pARO10 in the *LEU2* integrating plasmid

pLC605 (a gift from Leon Chan). To visualize the prospore membrane, we used a reporter consisting of amino acids 51 to 91 from Spo20 fused to the C terminus of link-yeGFP under control of pATG8 in a *LEU2* integrating plasmid (Sawyer et al., 2019). We also constructed a new variant with mKate2 in place of yeGFP. All *LEU2* integration constructs were integrated into the genome by cutting the plasmids with PmeI.

Sporulation conditions

Sporulation was induced using the traditional starvation method unless otherwise indicated. Diploid cells were first grown in YPD (1% yeast extract, 2% peptone, 2% glucose, 22.4 mg/L uracil, and 80 mg/L tryptophan) at room temperature for around 24 hours until the cultures reached a cell density of $OD_{600} \geq 10$. The cultures were then diluted in BYTA (1% yeast extract, 2% bacto tryptone, 1% potassium acetate, and 50 mM potassium phthalate) to $OD_{600} = 0.25$ and grown for 12-16 hours at 30°C. After reaching an $OD_{600} \geq 5$, the cells were pelleted, washed in sterile MilliQ water, and resuspended in the sporulation media SPO (0.5% or 1% potassium acetate, 0.02% raffinose, pH 7) to $OD_{600} = 1.85$. Meiotic cultures were shaken at 30°C for the duration of the experiment. At all stages, the flask size was 10 times the culture volume to ensure proper aeration.

To selectively enrich for the formation of dyads and triads, diploid cells were induced to sporulate in reduced carbon media (Eastwood and Meneghini, 2015). Cells were grown in YPD and BYTA as described above and then resuspended in SPO with reduced potassium acetate (0.1% potassium acetate, 0.02% raffinose, pH7) to an $OD_{600} = 1.85$.

After 5 hours at 30°C, the cells were then pelleted, washed in sterile MilliQ, and resuspended in 0.15% KCl.

Old cell isolation and sporulation

Old cells were enriched using a biotin-labeling and magnetic-sorting assay (Smeal et al., 1996). Cells were grown in YPD at room temperature or 30°C overnight until saturation ($OD_{600} \geq 10$) and then diluted to a cell density of $OD_{600} = 0.2$ in a new YPD culture. Cells were harvested before the cultures reached $OD_{600} = 1$ and were labeled with 8 mg/ml EZ-Link Sulfo-NHS-LC-biotin (ThermoFisher Scientific) for 30 minutes at 4°C. Biotinylated cells were grown for 6-8 generations in YPD at 30°C. Cells were subsequently harvested and mixed with 100 µl of anti-biotin magnetic beads (Miltenyi Biotechnology) for 15 minutes at 4°C. Cell were washed with PBS pH 7.4, 0.5% BSA buffer and sorted magnetically using LS depletion columns with a QuadroMacs sorter following the manufacturer's protocol. A fraction of the flow-through (biotin-negative) was kept as young cells and was budscar labeled with eluted old cells (biotin-positive) using 1 µg/ml Wheat Germ Agglutinin, Alexa Fluor™ 350 Conjugate (ThermoFisher Scientific). A mixture of old and young cells was subsequently washed twice in H_2O and once with SPO (0.5% or 1% potassium acetate, pH 7.0 + 0.02% raffinose). The cell mixture was resuspended with SPO at a cell density of $OD_{600} = 1.85$ and incubated at 30°C. The number of doublings in subsequent experiments was measured by counting the number of budscars.

Fluorescence Microscopy

Images were acquired using a DeltaVision Elite wide-field fluorescence microscope (GE Healthcare). Live cell images were generated using a 60x/1.42 NA oil-immersion objective; fixed cell images were generated using a 100x/1.40 NA oil-immersion objective. Specific imaging conditions for each experiment are indicated in Table S3. Images were deconvolved using softWoRx imaging software (GE Life Sciences). Unless otherwise noted, images were maximum intensity z-projected over the range of acquisition in FIJI (RRID:SCR_002285, Schindelin et al., 2012).

Live-cell imaging

Live cells were imaged in an environmental chamber heated to 30°C, using either the CellASIC ONIX Microfluidic Platform (EMD Millipore) or concanavalin A-coated, glass-bottom 96-well plates (Corning). All live imaging experiments used conditioned sporulation media (SPO filter-sterilized after five hours of sporulation at 30°C), as this was found to enhance meiotic progression. With the CellASIC system, cultures in SPO (OD_{600} = 1.85) were transferred to a microfluidic Y04D plate and were loaded with a pressure of 8 psi for 5 seconds. Conditioned SPO was subsequently applied with a constant flow rate of 10 µl/h for 15-20 hours. With the 96-well plates, cells were adhered to the bottom of the wells and 250 µl of conditioned SPO was added to each well. Images were acquired every 15 minutes for 15-18 hours.

Fixed-cell imaging

Fixed cells were prepared by treating 500-1000 µl of meiotic culture with 3.7% formaldehyde for 15 minutes at room temperature. Cells were permeabilized with either 1% Triton X-100 or 70% ethanol. Cells that were permeabilized in 1% Triton X-100 were processed in two different ways: 1) Cells were washed with 0.1 M potassium phosphate pH 6.4 and subsequently treated with 0.05 µg DAPI and 1% Triton in KPi sorbitol (0.1 M potassium phosphate, 1.2 M sorbitol, pH 7.5). Cells were then immediately washed with KPi sorbitol before imaging; or 2) Cells were treated for five minutes with 1% Triton in KPi sorbitol and then resuspended in KPi sorbitol. Cells were then adhered on a poly-lysine treated multi-well slide and mounted with Vectashield Mounting Medium with DAPI (Vector Labs). Cells that were permeabilized in 70% ethanol were washed with 0.1 M potassium phosphate pH 6.4 and then resuspended in KPi sorbitol buffer. Cells were then adhered to a poly-lysine treated multi-well slide, quickly permeabilized with 70% ethanol, and mounted with Vectashield Mounting Medium with DAPI (Vector Labs).

Electron microscopy

Yeast cells were concentrated by vacuum filtration onto a nitrocellulose membrane and then scrape-loaded into 50- or 100- µm-deep high pressure freezing planchettes (McDonald and Muller-Reichert, 2002). Freezing was done in a Bal-Tec HPM-010 high-pressure freezer (Bal-Tec AG).

High pressure frozen cells stored in liquid nitrogen were transferred to cryovials containing 1.5 ml of fixative consisting of 1% osmium tetroxide, 0.1% uranyl acetate, and 5% water in acetone at liquid nitrogen temperature (-195˚C) and processed for

freeze substitution according to the method of McDonald and Webb (McDonald, 2014; McDonald and Webb, 2011). Briefly, the cryovials containing fixative and cells were transferred to a cooled metal block at -195˚C; the cold block was put into an insulated container such that the vials were horizontally oriented, and shaken on an orbital shaker operating at 125 rpm. After 3 hours the block and cryovials had warmed to 20˚C and were transitioned to resin infiltration.

Resin infiltration was accomplished by a modification of the method of McDonald (McDonald, 2014). Briefly, cells were rinsed 4-5 times in pure acetone and infiltrated with Epon-Araldite resin in increasing increments of 25% over 3 hours plus 3 changes of pure resin at 30 minutes each. Cells were removed from the planchettes at the beginning of the infiltration series and spun down at 6,000 x g for 1 minute between solution changes. The cells in pure resin were placed in between 2 PTFE-coated microscope slides and polymerized over 2 hours in an oven set to 100˚C.

Cells were cut out from the thin layer of polymerized resin and remounted on blank resin blocks for sectioning. Serial sections of 75 nm were cut on a Reichert-Jung Ultracut E microtome and picked up on 1 x 2 mm slot grids covered with a 0.6% Formvar film. Sections were post-stained with 1% aqueous uranyl acetate for 10 minutes and lead citrate for 10 minutes (Reynolds, 1963). Images of cells on serial sections were taken on an FEI Tecnai 12 electron microscope operating at 120 kV equipped with a Gatan Ultrascan 1000 CCD camera.

Models were constructed from serial sections with the IMOD package (Kremer et al., 1996), using 3DMOD version 4.9.8. Initial alignment was performed using the Midas tool in the ETomo interface of the IMOD package; afterwards, sections were rotated and minorly warped in Midas to improve alignment. The plasma membrane, nuclear envelope, and nucleoli were segmented in IMOD by manual tracing using the Drawing Tools plugin created by Andrew Noske. Movies were made in 3DMOD and assembled in QuickTime Pro Version 7.6.6.

Image quantification

To quantify the percentage of Nsr1 sequestration, measurements of Nsr1-GFP signal intensity were taken with Fiji (RRID:SCR_002285, Schindelin et al., 2012) from maximum intensity z-projection movies of young and old cells that eventually formed tetrads. Nsr1 signal was measured after nucleolus segregation to the four dividing nuclei, determined by the appearance of four Nsr1 foci in the four nuclei. Percent sequestration was measured by calculating the raw integrated intensity in the fifth compartment and dividing it by the sum of the signal present in the four nuclei and the fifth compartment. The mean intensity measured from non-cellular background was subtracted in each field of view before quantifying Nsr1 levels.

For the vacuolar lysis experiments, the timing of vacuolar membrane disruption and either excluded nucleoporin or protein aggregate disappearance were scored in cells that eventually became tetrads. Vacuolar membrane disruption was defined as the time point at which Vph1 signal becomes diffuse, instead of localizing to the membrane. In

less than 25% of cells, the vacuole appeared to crumple and collapse over more than an hour prior to vacuolar membrane disappearance. Since we were unable to interpret these changes in vacuolar morphology, these cells were not included in our quantification. Protein aggregate and NPC disappearance was defined as the time point at which the excluded fluorescence signal was no longer visible.

For protein aggregate and nucleolar sequestration experiments, sequestration was scored in WT cells that formed tetrads and *spo21Δ* cells that progressed through anaphase II, as tetrad formation cannot be assessed in *spo21Δ* cells. Protein aggregate sequestration was scored in old cells and was defined as the aggregate no longer associating with chromatin after the four anaphase II nuclei became distinct. Nucleolar sequestration was scored in young cells and was defined as the presence of a fifth focus that did not associate with a gamete nucleus after the four anaphase II nuclei became distinct.

Immunoblotting

For each meiotic time point, 3.7 OD_{600} equivalents of cells were pelleted and resuspended in 2 mL of 5% trichloroacetic acid and incubated at 4°C for ≥ 10 minutes. The cells were subsequently washed with 1 mL 10 mM Tris pH 8.0 and then 1 mL of acetone, before being left to dry overnight. Then, ~100 µl glass beads and 100 µl of lysis buffer (50 mM Tris-HCl pH 8.0, 1 mM EDTA, 15 mM Tris pH 9.5, 3 mM DTT, 1X cOmplete EDTA-free inhibitor cocktail [Roche]) were added to each dried pellet. Protein

extracts were generated by pulverization using a Mini-Beadbeater-96 (BioSpec). The samples were then treated with 50 µl of 3X SDS sample buffer (187.5 mM Tris pH 6.8, 6% β-mercaptoethanol, 30% glycerol, 9% SDS, 0.05% bromophenol blue) and heated at 37˚C for 5 minutes.

Proteins were separated by polyacrylamide gel electrophoresis using 4–12% Bis-Tris Bolt gels (Thermo Fisher) and transferred onto nitrocellulose membranes (0.45 µm, Bio-rad, Hercules, CA). The Nup84-GFP blot was generated using a semi-dry transfer apparatus (Trans-Blot Turbo Transfer System, Bio-Rad). The Nup170-GFP blot was generated using a Mini-PROTEAN Tetra tank (Bio-Rad) filled with 25 mM Tris, 195 mM glycine, and 15% methanol, run at 180 mA (max 80 V) for 3 hours at 4°C. The membranes were blocked for at least 30 minutes with Odyssey PBS Blocking Buffer (LI-COR Biosciences) at room temperature. The blots were incubated overnight at 4°C with a mouse anti-GFP antibody (RRID:AB_2323808, 63281, Clontech) at a 1:2,000 dilution in blocking buffer. As a loading control, we monitored Hxk2 levels using a rabbit anti-hexokinase antibody (RRID:AB_219918, 100-4159, Rockland) at a 1:10,000 dilution in blocking buffer. Membranes were washed in PBST (PBS with 0.1% Tween-20) and incubated with an anti-mouse secondary antibody conjugated to IRDye 800CW at a 1:15,000 dilution (RRID:AB_621847, 926–32212, LI-COR Biosciences) and an anti-rabbit antibody conjugated to IRDye 680RD at a 1:15,000 dilution (RRID:AB_10956166, 926–68071, LI-COR Biosciences) to detect the GFP epitope and Hxk2, respectively. Immunoblot images were generated using the Odyssey CLX system (LI-COR Biosciences).

Data availability

All the reagents generated in this study are available upon request.

Acknowledgments: We thank Gloria Brar, Andy Dillin, Rebecca Heald, Jasper Rine, James Olzmann, Jingxun Chen, Amy Tresenrider, Eric Sawyer, Tina Sing, Victoria Jorgensen, Amy Eisenberg, Helen Vander Wende, and Isaiah Thomas for comments on this manuscript. This work was supported by funds from the Pew Charitable Trusts (00027344), Damon Runyon Cancer Research Foundation (35-15), National Institutes of Health (DP2 AG055946-01), and Glenn Foundation for Medical Research to EÜ; a National Science Foundation Graduate Research Fellowship (DGE 1752814) and National Institutes of Health Traineeship (T32 GM007232) to GAK; and a National Institutes of Health F31 Fellowship (F31AG060656) and National Institutes of Health Traineeship (T32 GM007127-41) to JSG. The content is solely the responsibility of the authors and does not necessarily represent the official views of the National Institutes of Health. We thank Reena Zalpuri, Guangwei Min, and the University of California, Berkeley, Electron Microscope Lab for assistance in electron microscopy sample preparation and data collection. We acknowledge technical support from Eric Sawyer, Yuzhang Chen, and George Otto.

The authors declare no competing financial interests.

Author contributions: Elçin Ünal, Grant King, and Jay Goodman designed research. Grant King, Jay Goodman, Keerthana Chetlapalli, and Jennifer Schick performed experiments. Grant King, Jay Goodman, Keerthana Chetlapalli, Jennifer Schick, and Elçin Ünal analyzed data. Grant King, Danielle Jorgens, Kent McDonald performed the electron microscopy experiments. Grant King, Jay Goodman, and Elçin Ünal wrote the manuscript.

FIGURE LEGENDS

Figure 1. Senescence factors are sequestered away from chromosomes in meiosis II and are subsequently eliminated. A. Schematic depiction of a young and old budding yeast cell. **B.** (left panel) Montage of a young cell (1 generation old) with diffuse Hsp104-GFP progressing through meiosis (UB9724). (right panel) Montage of an aged cell (7 generations old) containing protein aggregates labeled with Hsp104-GFP progressing through meiosis (UB9724). Chromosomes were visualized with histone marker Htb1-mCherry. **C.** (left panel) Montage of a young cell (0 generations old) with rDNA repeats, visualized with TetR-GFP binding to tetO arrays in the rDNA repeats, progressing through meiosis (UB17338). (right panel) Montage of an aged cell (9 generations old) containing rDNA circles, visualized with TetR-GFP binding to tetO arrays in the rDNA repeats, progressing through meiosis. (UB17338). Chromosomes were visualized with histone marker Hta1-mApple. For B-C, the time point depicting anaphase II onset was defined as 0 minutes as indicated by the arrows. **D.** Quantification depicting the timing of protein aggregate sequestration relative to the timing of anaphase II onset (median replicative age = 7, mean replicative age = 6.3 ± 1.5, n = 50 cells). **E.** Quantification depicting the timing of rDNA circle sequestration relative to the timing of anaphase II onset (median replicative age = 8, mean replicative age = 8.2 ± 2.4, n = 50 cells). Scale bars, 2 µm.

Figure 2. Nucleolar material is sequestered away from chromosomes during meiosis II in young and aged cells. A. Montage of a young cell (1 generation old) with the nucleolar tag Nsr1-GFP progressing through meiosis (UB16712). **B.** Montage of an aged cell (9 generations old) containing abnormal nucleolar material, labeled with Nsr1-GFP, progressing through meiosis (UB16712). For A-B, chromosomes were visualized with the histone marker Htb1-mCherry and the time point depicting anaphase II onset was defined as 0 minutes as indicated by the arrows. **C.** Quantification depicting timing of Nsr1 sequestration relative to timing of anaphase II onset (median replicative age = 8, mean replicative age = 7.2 ± 2.4, n = 50 cells). **D.** Quantification depicting the degree of Nsr1 sequestration in cells of different ages (n = 50 for cells with 0-4 doublings, n = 53 for cells with 5-8 doublings, and n = 49 for cells with 9 or more doublings). The Mann-Whitney nonparametric test was used to test statistical significance, and data were generated from two biological replicates. **E.** Montage of an aged cell (9 generations old) with the nucleolus marked by Nsr1-GFP and protein aggregates marked by Hsp104-mCherry aggregates progressing through meiosis (UB13299). For E, the time point depicting Nsr1-GFP sequestration was defined as 0 minutes as indicated by the arrow. **F.** Quantification depicting the frequency of sequestered Hsp104-mCherry aggregates localizing adjacent to sequestered Nsr1-GFP (UB13299) immediately after nucleolar segregation (median replicative age = 7, mean replicative age = 6.7 ± 1.5, n = 100 cells). Adjacency was defined as sequestered Nsr1-GFP signal either neighboring or exhibiting partial overlap with sequestered Hsp104-mCherry signal in individual z-sections. Scale bars, 2 µm.

Figure 3. Nucleoporins from the core of the nuclear pore complex, but not the nuclear basket, are sequestered away from chromosomes during meiosis II and subsequently eliminated. **A.** A schematic depicting the different nucleoporins and subcomplexes that comprise the nuclear pore complex (NPC), adapted from (Rajoo et al., 2018). Nucleoporins marked with an asterisk are sequestered away from chromosomes; nucleoporins marked with a pound sign return to dividing nuclei. For each nucleoporin, the observed phenotype was observed in all tetrads examined (n ≥ 25 tetrads). **B-G.** Montages of cells with tagged nucleoporins from each NPC subcomplex progressing through meiosis. Chromosomes were visualized with the histone marker Htb1-mCherry, and the first time point depicting anaphase II was defined as 0 minutes as indicated by the arrows. **B.** Nup170-GFP, an inner ring complex nucleoporin (UB11513) **C.** Nup120-GFP, a Y-complex nucleoporin (UB13499) **D.** Pom34-GFP, a transmembrane nucleoporin (UB13503) **E.** Nup82-GFP, a cytoplasmic filament nucleoporin (UB14652) **F.** Nup49-GFP, a channel nucleoporin (UB13509) **G.** Nup2-GFP, a nuclear basket nucleoporin (UB15305) **H.** Montage depicting localization of Nup2-GFP, a nuclear basket nucleoporin, and Nup49-mCherry, a channel nucleoporin (UB15672). Scale bars, 2 µm.

Figure 4. Age-dependent nuclear damage is sequestered with disposed NPCs during anaphase II. A. Montage of an aged cell (7 generations old) with protein aggregates, labeled with Hsp104-mCherry, and NPCs, labeled Nup170-GFP, progressing through meiosis (UB12975). **B.** Montage of an aged cell (9 generations old) with rDNA circles, marked by TetR-GFP binding to tetO arrays in the rDNA repeats, and NPCs, labeled with Nup49-mCherry, progressing through meiosis **C.** Montage of an aged cell (7 generations old) with abnormal nucleolar material, marked by Nsr1-GFP, and NPCs, marked by Nup49-mCherry, progressing through meiosis (UB16708). The first time point depicting NPC sequestration was defined as 0 minutes as indicated by the arrows. Scale bar, 2 µm.

Figure 5. Nucleoporins are sequestered to a nuclear envelope-bound compartment during meiosis II. A-B. Maximum intensity projections of fixed young cells depicting the localization of inner nuclear membrane proteins – **A.** Heh1-3xeGFP (UB14391) and **B.** the synthetic construct eGFP-h2NLS-L-TM from (Meinema et al., 2011) (UB12932) – relative to the nucleoporin Nup49-mCherry and DAPI. Scale bars, 2 µm. **C-D.** Reconstructions of **C.** a young late anaphase II cell and **D.** a young post-meiosis II cell from 70 nm serial TEM micrographs. Gamete plasma membranes are depicted in magenta, the nuclear envelope is depicted in cyan, and nucleoli are depicted in yellow. Scale bars, 0.5 µm. **E-F.** Electron micrographs of **E.** a young late anaphase II cell and **F.** a young post-meiosis II cell with insets depicting the nuclear envelope-bound region outside the gamete plasma membranes. Solid arrows indicate NPCs; dashed arrows indicate nucleolar mass. Note that the electron micrographs in panel F come from the cell reconstructed in panel D. Scale bars, 0.5 µm.

Figure 6. Core nucleoporins and age-dependent damage are excluded from developing gametes during meiosis II. A. Maximum intensity projections over 6 µm of fixed young cells depicting localization of the gamete plasma membrane marker GFP-Spo20$^{51-91}$ relative to the nucleoporin Nup49-mCherry and DAPI (UB12342). **B.** Maximum intensity projections over 8 µm of fixed young cells (UB12436) depicting localization of the leading edge complex tag Don1-GFP relative to the nucleoporin Nup49-mCherry and DAPI. **C-D.** Montages of cells with a protein aggregate tag, Hsp104-mCherry, and a marker of the gamete plasma membrane, GFP-Spo20$^{51-91}$ (UB11821). **C.** An aged cell (6 generations old) that excluded its protein aggregate from developing gametes. **D.** An aged cell (6 generations old) that failed to exclude its protein aggregate from developing gametes. For C-D, the first time point depicting gamete plasma membrane nucleation was defined as 0 minutes as indicated by the arrows. Scale bars, 2 µm.

Figure 7. Core nucleoporins and protein aggregates are turned over coincident with vacuolar lysis. A. Montage of a young cell with an inner ring complex nucleoporin tag, Nup170-GFP, and a marker for the vacuole, Vph1-mCherry (UB15890). Images are maximum intensity projections over 6 µm; the first time point depicting Nup170 disappearance was defined as 0 minutes as indicated by the arrow. **B.** Quantification of the experiment in panel A. Timing of the excluded Nup170-GFP disappearance relative to vacuolar lysis (n = 140 cells). **C.** Montage of an aged cell (8 generations old) with a protein aggregate

tag, Hsp104-mCherry, and a marker for the vacuolar membrane, Vph1-GFP (UB12163). Images are maximum intensity projections over 8µm; the first time point depicting Hsp104 foci disappearance was defined as 0 minutes as indicated by the arrow. **D.** Quantification of the experiment in panel C. Timing of excluded Hsp104-mCherry disappearance relative to vacuolar lysis. (median replicative age = 6, mean replicative age = 5.9 ± 1.5, n = 100 cells). For panels A and C, solid arrows indicate the intact vacuolar membrane of mother cell and dashed arrows indicate vacuolar permeabilization. For panels B and D, vacuolar lysis was scored as the time of vacuolar membrane disappearance. Scale bars, 2 µm. Immunoblot assay measuring degradation of **E.** Nup84-GFP in wild type (UB13497) and *ndt80Δ* cells (UB19929) **F.** Nup170-GFP in wild type (UB11513) and *ndt80Δ* cells (UB19927). Hxk2 levels were measured as a loading control.

Figure 8. Gamete plasma membrane development is necessary for nucleoporin sequestration. A. Montage of inner ring complex nucleoporin Nup170 localization relative to Htb1-mCherry in a young *spo21Δ* cell (UB13377). The first time point depicting anaphase II was defined as 0 minutes as indicated by the arrow. **B.** Quantification of the experiment in panel A for *spo21Δ* and Figure 3B for WT. Number of nuclei enriched for nucleoporins following anaphase II in WT or *spo21Δ* cells. (n = 108 cells for WT, n = 118 cells *spo21Δ*). **C-D.** Maximum intensity projections of fixed young cells depicting **C.** gamete plasma membrane GFP-Spo20$^{51-91}$ (UB12342) or **D.** leading edge Don1-GFP (UB12436) localization relative to nucleoporin Nup49-mCherry localization in low-carbon conditions that promoted the formation of fewer than four gamete plasma membranes. **E.** Quantification of the experiment in panel C. Number of nuclei enriched for nucleoporins following anaphase II in cells with variable numbers of gamete plasma membranes (4 PSMs: n = 48; 3 PSMs: n = 80; 2 PSMs: n = 46). **F.** Maximum intensity projections of fixed young cells showing gamete plasma membrane (GFP-Spo20$^{51-91}$) and nucleoporin (Nup49-mCherry) localization in mutants defective in leading edge complex formation, *ssp1Δ* (UB13473) or *ady3Δ irc10Δ* (UB13583). Arrowheads on merged images denote location of DAPI constrictions. Scale bars, 2 µm.

Figure 9. **Protein aggregate and nucleolar sequestration is coupled to NPC sequestration via gamete plasma membrane development**. **A**. Montages of aged *spo21Δ* cells in which protein aggregates marked by Hsp104-GFP were either (left panel) sequestered (5 generations old) or (right panel) retained (6 generations old) by chromosomes during anaphase II (UB14418). **B.** Quantification of cells retaining protein aggregates in WT (UB9724) and *spo21Δ* cells (UB14418). Median replicative age = 7, mean replicative age = 6.5 ± 1.5, n = 100 for WT cells; median replicative age = 6, mean replicative age = 6.2 ± 1.2, n = 100 for *spo21Δ* cells. **C.** Montages of young *spo21Δ* cells in which nucleolar material was either (left panel) sequestered or (right panel) retained by chromosomes during anaphase II (UB 14419). **D.** Quantification of cells retaining Nsr1 in WT (UB15118) and *spo21Δ* cells (UB14419). n = 100 for WT cells, n = 100 for *spo21Δ* cells. For A and C chromosomes were visualized with the histone marker Htb1-mCherry. For A the first time point depicting protein aggregate sequestration or retention was defined as 0 minutes as indicated by the arrows. For C, the first time point depicting nucleolar sequestration or retention was defined as 0 minutes as indicated by the arrows. Scale bars, 2 µm.

Figure 10. Nuclear rejuvenation during meiosis. Old yeast cells accumulate nuclear damage including extrachromosomal rDNA circles (red), nuclear-associated protein aggregates (brown), abnormal and enlarged nucleoli (yellow), and damaged long-lived proteins including nucleoporins (green). During meiosis II, a nuclear envelope-bound compartment containing much of this age-associated damage is formed and remains outside of the developing gametes. The material in the excluded compartment is turned over coincident with vacuolar lysis, completing rejuvenation of the gamete nuclei. Sequestration of the age-dependent damage away from gamete nuclei requires proper gamete plasma membrane development during anaphase II.

Figure 1 - Supplement 1. Age-induced protein aggregates are localized inside the nucleus prior to the meiotic divisions. A. Z-slices of an aged prophase I cell (7 generations old) depicting localization of NPCs, marked by Nup170-GFP, and protein aggregates, marked by Hsp104-mCherry (UB12975). **B.**

Quantification depicting frequency of pre-meiotic cells with protein aggregates inside the nucleus (median replicative age = 6, mean replicative age = 6.2 ± 2.1, n =100 cells). Scale bars, 2 µm.

Figure 1 - Supplement 2. Supplement 1. TetR-GFP is not sequestered in aged cells lacking the rDNA-tetO array Montage of an aged cell (9 generations old) containing TetR-GFP but lacking the tetO array (UB17509). Chromosomes were visualized with histone marker Hta1-mApple, and the time point depicting anaphase II onset was defined as 0 minutes as indicated by the arrow. Scale bars, 2 µm.

Figure 3 – Supplement 1. The inner ring complex nucleoporins Nup188 and Nup53 are sequestered away from chromosomes and subsequently eliminated. A-B. Montages of young cells with **A.** Nup188-GFP (UB13505) and **B.** Nup53-GFP (UB3810) progressing through meiosis. Chromosomes were visualized with the histone marker Htb1-mCherry, and the time point depicting anaphase II onset was defined as 0 minutes as indicated by the arrows. Scale bars, 2 µm.

Figure 3 – Supplement 2. The Y-complex nucleoporin Nup84 is sequestered away from chromosomes and subsequently eliminated. Montages of a young cell with Nup84-GFP (UB13497) progressing through meiosis. Chromosomes were visualized with the histone marker Htb1-mCherry, and the time point depicting anaphase II onset was defined as 0 minutes as indicated by the arrow. Scale bar, 2 µm.

Figure 3 – Supplement 3. The transmembrane nucleoporin Ndc1 is sequestered away from chromosomes and subsequently eliminated. Montages of a young cell with Ndc1-GFP (UB15301) progressing through meiosis. Chromosomes were visualized with the histone marker Htb1-mCherry, and the time point depicting anaphase II onset was defined as 0 minutes as indicated by the arrow. Scale bar, 2 µm.

Figure 3 – Supplement 4. The cytoplasmic filament nucleoporin Nup159 is sequestered away from chromosomes and subsequently eliminated. Montages of a young cell with Nup159-GFP (UB14650) progressing through meiosis. Chromosomes were visualized with the histone marker Htb1-mCherry, and the time point depicting anaphase II onset was defined as 0 minutes as indicated by the arrow. Scale bar, 2 µm.

Figure 3 – Supplement 5. The channel nucleoporin Nup57 is sequestered away from chromosomes and subsequently eliminated. Montages of a young cell with Nup57-GFP (UB14654) progressing through meiosis. Chromosomes were visualized with the histone marker Htb1-mCherry, and the time point depicting anaphase II onset was defined as 0 minutes as indicated by the arrow. Scale bar, 2 µm.

Figure 3 – Supplement 6. The nuclear basket nucleoporins Nup1 and Nup60 return to dividing nuclei during and after anaphase II. A-B. Montages of young cells with **A.** Nup1-GFP (UB15303) and **B.** Nup60-GFP (UB14646) progressing through meiosis. Chromosomes were visualized with the histone marker Htb1-mCherry, and the time point depicting anaphase II onset was defined as 0 minutes as indicated by the arrows. Scale bars, 2 µm.

Figure 4 - Supplement 1. Protein aggregates are sequestered with disposed NPCs in fixed cells. Maximum intensity projections of fixed premeiotic and meiotic cells depicting localization of NPCs and protein aggregates. Protein aggregates, marked by Hsp104-mCherry, co-localized with sequestered NPCs, marked by Nup170-GFP, during meiosis II (UB12975). Scale bar, 2 µm.

Figure 4 - Supplement 2. Nucleolar material is sequestered with disposed NPCs in fixed cells. Maximum intensity projections of fixed premeiotic and meiotic cells depicting localization of NPCs and nucleolar material. Nucleolar material, marked by Nsr1-GFP, co-localized with sequestered NPCs, marked by Nup49-mCherry, during meiosis II (UB16708). Scale bar, 2 µm.

Figure 5 - Supplement 1. The inner nuclear envelope protein Heh1 localizes to the dividing nuclei and nucleoporin mass during anaphase II. A-B. Montages of young cells with a fluorescently-tagged inner nuclear membrane protein Heh1-3xGFP and either **A.** Htb1-mCherry, a histone marker (UB14393), or **B.** Nup49-mCherry, a nucleoporin (UB14391). The time point depicting anaphase II onset was defined as 0 minutes as indicated by the arrows. Scale bars, 2 µm.

Figure 5 - Supplement 2. The nuclear envelope region outside of gamete plasma membranes contains NPCs and nucleolar material during early anaphase II. Electron micrographs of a young early anaphase II cell and an inset of the nuclear envelope-bound region outside the gamete plasma membranes. Solid arrows indicate NPCs; dashed arrows indicate nucleolar mass. Scale bars, 0.5 µm.

Figure 6 – Supplement 1. Dynamic localization of sequestered nucleoporins relative to gamete plasma membranes. A-B. Montages of young cells progressing through the meiotic divisions with a gamete plasma membrane marker GFP-Spo20$^{51-91}$ and either **A.** a histone marker Htb1-mCherry (UB12434), or **B.** a nucleoporin marker Nup49-mCherry (UB12342). The time point depicting anaphase II onset was defined as 0 minutes as indicated by the arrows. Scale bars, 2 µm.

Figure 6 – Supplement 2. Dynamic localization of sequestered nucleoporins relative to the leading edge of gamete plasma membranes. A-B. Montages of young cells progressing through the meiotic divisions with the leading edge marker Don1-GFP and either **A.** a histone marker Htb1-mCherry (UB12438), or **B.** a nucleoporin marker Nup49-mCherry (UB12436). The time point depicting anaphase II onset was defined as 0 minutes as indicated by the arrows. Scale bars, 2 µm.

Figure 6 – Supplement 3. Nucleolar material in aged cells is excluded from the developing gametes. Montage of an aged cell (7 generations old) excluding nucleolar material marked by Nsr1-GFP during meiosis II (UB16710). Gamete plasma membranes were marked by mKate-Spo20$^{51-91}$. The time point depicting anaphase II onset was defined as 0 minutes as indicated by the arrow. Scale bar, 2 µm.

Figure 8 – Supplement 1. The leading edge complex member Ssp1 is required for proper gamete plasma membrane formation and nucleoporin sequestration. A-C. Montages of young *ssp1Δ* cells progressing through the meiotic divisions with the following tags: **A.** nucleoporin Nup170-GFP and histone Htb1-mCherry (UB13373); **B.** gamete plasma membrane GFP-Spo20$^{51-91}$ and histone Htb1-mCherry (UB13475); **C.** and gamete plasma membrane GFP-Spo20$^{51-91}$ and nucleoporin Nup49-mCherry (UB13473). The time point depicting anaphase II onset was defined as 0 minutes as indicated by the arrows. Scale bars, 2 µm.

Figure 8 – Supplement 2. The leading edge complex members Ady3 and Irc10 are required for proper gamete plasma membrane formation and nucleoporin sequestration. A-C. Montages of young *ady3Δ irc10Δ* cells progressing through the meiotic divisions with the following tags: **A.** nucleoporin Nup170-GFP and histone Htb1-mCherry (UB12465); **B.** gamete plasma membrane GFP-Spo20$^{51-91}$ and histone Htb1-mCherry (UB13585); **C.** and gamete plasma membrane GFP-Spo20$^{51-91}$ and nucleoporin Nup49-mCherry (UB13583). The time point depicting anaphase II onset was defined as 0 minutes as indicated by the arrows. Scale bars, 2 µm.

Figure 9 – Supplement 1. Protein aggregates localize to NPCs during anaphase II in *spo21Δ* cells. A-B. Protein aggregates, labeled with Hsp104-mCherry, in aged *spo21Δ* cells co-localize with NPCs, marked by Nup170-GFP (UB13568). **A.** Montage of an aged *spo21Δ* cell (7 generations old) sequestering protein aggregates during meiosis II. **B.** Montage of an aged *spo21Δ* cell (6 generations old) retaining protein aggregates during meiosis II. For A-B, the time point depicting anaphase II was defined as 0 minutes as indicated by the arrows. Scale bars, 2 µm.

Figure 9 – Supplement 2. Nucleolar material localizes to NPCs during anaphase II in *spo21Δ* cells. **A-B.** Nucleolar material in young *spo21Δ* cells co-localizes with NPCs marked by Nup49-mCherry in *spo21Δ* cells (UB14425). **A.** Montage of a young *spo21Δ* cell sequestering an Nsr1-GFP punctum during meiosis II. **B.** Montage of a young *spo21Δ* cell retaining all Nsr1-GFP during meiosis II. For A-B, the time point depicting anaphase II was defined as 0 minutes as indicated by the arrows. Scale bars, 2 µm.

Video 1. Protein aggregates are sequestered away from chromosomes during meiosis II and subsequently eliminated. An aged cell (7 generations old) with protein aggregates undergoing gametogenesis as depicted in Figure 1B. Protein aggregates were followed with Hsp104-GFP and meiotic staging was followed using a histone marker Htb1-mCherry (UB9724). Movie frame rate, 4 frames per second. Scale bar, 2 µm.

Video 2. rDNA circles are sequestered away from chromosomes during meiosis II and subsequently eliminated. An aged cell (9 generations old) containing tetO arrays in rDNA repeats undergoing gametogenesis as depicted in Figure 1C. rDNA was visualized with TetR-GFP and meiotic staging was followed using a histone marker Hta1-mApple (UB17338). Movie frame rate, 4 frames per second. Scale bar, 2 µm.

Video 3. Abnormal nucleolar material is sequestered away from chromosomes during meiosis II and subsequently eliminated. An aged cell (9 generations old) with abnormal nucleolar material undergoing gametogenesis as depicted in Figure 2A. Nucleoli were followed with Nsr1-GFP and meiotic staging was followed using a histone marker Htb1-mCherry (UB16712). Movie frame rate, 4 frames per second. Scale bars, 2 µm.

Video 4. Core nucleoporins are sequestered away from chromosomes during meiosis II and subsequently eliminated. A young cell with a tagged inner ring complex nucleoporin, Nup170-GFP, during gametogenesis as depicted in Figure 3B (UB11513). Meiotic staging was followed using a histone marker, Htb1-mCherry. Movie frame rate, 4 frames per second. Scale bars, 2 µm.

Video 5. Nuclear basket nucleoporins are not sequestered with core nucleoporins during meiosis II. A young cell with a tagged nuclear basket nucleoporin, Nup2-GFP, and a tagged channel nucleoporin, Nup49-mCherry, during gametogenesis as depicted in Figure 3H (UB15672). Movie frame rate, 4 frames per second. Scale bars, 2 µm.

Video 6. A nuclear envelope-bound compartment remains outside of developing gametes during meiosis II. Serial TEM micrographs of a young cell during late meiosis II used to construct the model shown in Figure 5C (UB11513). Section thickness, 70 nm. Scale bars, 0.5 μm.

Video 7. A nuclear envelope-bound compartment remains outside of developing gametes during meiosis II. Reconstruction of a young cell during late meiosis II from 70 nm serial TEM micrographs as depicted in Figure 5C (UB11513). Plasma membranes are depicted in magenta, the nuclear envelope is depicted in cyan, and nucleoli are depicted in yellow. Scale bars, 0.5 μm.

Video 8. A nuclear envelope-bound compartment remains outside of gametes during gamete development. Serial TEM micrographs of a young cell during gamete development used to construct the model shown in Figure 5D (UB11513). Section thickness, 70 nm. Scale bars, 0.5 μm.

Video 9. A nuclear envelope-bound compartment remains outside of gametes during gamete development. Reconstruction of a young cell during gamete development from 70 nm serial TEM micrographs as depicted in Figure 5D (UB11513). Plasma membranes are depicted in magenta, the nuclear envelope is depicted in cyan, and nucleoli are depicted in yellow. Scale bars, 0.5 μm.

Video 10. Protein aggregates excluded from developing gametes are eliminated. An aged cell (6 generations old) with protein aggregates undergoing gametogenesis as depicted in Figure 6B. Protein aggregates were followed with Hsp104-mChery and gamete plasma membrane formation was followed using GFP-Spo20$^{51-91}$ (UB11821). Movie frame rate, 4 frames per second. Scale bars, 2 µm.

Video 11. Protein aggregates inherited by developing gametes are not eliminated. An aged cell (6 generations old) with protein aggregates undergoing gametogenesis as depicted in Figure 6C. Protein aggregates were followed with Hsp104-mCherry and gamete plasma membrane formation was followed using GFP-Spo20$^{51-91}$ (UB11821). Movie frame rate, 4 frames per second. Scale bars, 2 µm.

Video 12. Core nucleoporins are eliminated coincident with vacuolar lysis. A young cell with an inner ring complex nucleoporin tag, Nup170-GFP, and a marker for the vacuole, Vph1-mCherry, undergoing gametogenesis as depicted in Figure 7A (UB15890). Movie frame rate, 4 frames per second. Scale bars, 2 µm.

Video 13. Protein aggregates are eliminated coincident with vacuolar lysis. An aged cell (8 generations old) with protein aggregates undergoing gametogenesis as depicted in Figure 7C. Protein aggregates were followed with Hsp104-mCherry and vacuolar lysis was followed using vacuolar membrane marker Vph1-GFP (UB12163). Movie frame rate, 4 frames per second. Scale bars, 2 µm.

Video 14. Gamete plasma membrane development is necessary for nucleoporin sequestration. A young *spo21Δ* cell with inner ring complex nucleoporin tag Nup170-GFP and histone marker Htb1-mCherry undergoing gametogenesis as depicted in Figure 8A (UB13377). Movie frame rate, 4 frames per second. Scale bars, 2 µm.

Table S1. Strain table.

Table S2. Primers used for strain construction.

Table S3. Plasmids used for strain construction.

Table S4. Imaging conditions. Transmission, exposure time, and excitation/emission wavelengths are specified for each channel. Distance between z-sections and number of z-sections acquired are indicated.

Table S5. Meiotic septin and leading edge complex genes are not required for nuclear pore complex sequestration. Movies of strains with the indicated deletion, a meiotic staging marker (Htb1-GFP), and either (1) a fluorescently tagged inner ring complex nucleoporin (Nup170-GFP) or (2) a fluorescently tagged chaperone that marks age-induced protein aggregates (Hsp104-GFP) were generated. For mutants with successful spore packaging, at least 25 tetrads were observed. For mutants with poor or unsuccessful spore packaging, at least 50 cells that proceeded through MII were observed and compared to wild type (UB11513 for Nup170-GFP; UB11821 for Hsp104-GFP).

REFERENCES

1. Aguilaniu, H., Gustafsson, L., Rigoulet, M., and Nystrom, T. (2003). Asymmetric inheritance of oxidatively damaged proteins during cytokinesis. Science *299*, 1751-1753.
2. Beck, M., and Hurt, E. (2017). The nuclear pore complex: understanding its function through structural insight. Nat Rev Mol Cell Biol *18*, 73-89.
3. Bohnert, K.A., and Kenyon, C. (2017). A lysosomal switch triggers proteostasis renewal in the immortal C. elegans germ lineage. Nature *551*, 629-633.
4. Boselli, M., Rock, J., Unal, E., Levine, S.S., and Amon, A. (2009). Effects of age on meiosis in budding yeast. Developmental cell *16*, 844-855.
5. Brar, G.A., Yassour, M., Friedman, N., Regev, A., Ingolia, N.T., and Weissman, J.S. (2012). High-resolution view of the yeast meiotic program revealed by ribosome profiling. Science *335*, 552-557.
6. Brewer, B.J., Zakian, V.A., and Fangman, W.L. (1980). Replication and meiotic transmission of yeast ribosomal RNA genes. Proc Natl Acad Sci U S A *77*, 6739-6743.
7. Byers, B. (1981). Cytology of the yeast life cycle. In The Molecular Biology of the Yeast Saccharomyces: Life Cycle and Inheritance, J.N. Strathern, E.W. Jones, and J.R. Broach, eds. (Cold Spring Harbor, NY: Cold Spring Harbor Laboratory Press), pp. 59-96.
8. Cabrera, M., Novarina, D., Rempel, I.L., Veenhoff, L.M., and Chang, M. (2017). A simple microfluidic platform to study age-dependent protein abundance and localization changes in Saccharomyces cerevisiae. Microb Cell *4*, 169-174.
9. Carlile, T.M., and Amon, A. (2008). Meiosis I is established through division-specific translational control of a cyclin. Cell *133*, 280-291.
10. Caudron, F., and Barral, Y. (2009). Septins and the lateral compartmentalization of eukaryotic membranes. Developmental cell *16*, 493-506.
11. Cheng, Z., Otto, G.M., Powers, E.N., Keskin, A., Mertins, P., Carr, S.A., Jovanovic, M., and Brar, G.A. (2018). Pervasive, Coordinated Protein-Level Changes Driven by Transcript Isoform Switching during Meiosis. Cell *172*, 910-923.e916.
12. Chu, D.B., and Burgess, S.M. (2016). Nonessential nucleoporins Nup2, Nup60 and Nup84 are required for normal meiosis in *Saccharomyces cerevisiae*. bioRxiv, 054791.
13. Clay, L., Caudron, F., Denoth-Lippuner, A., Boettcher, B., Buvelot Frei, S., Snapp, E.L., and Barral, Y. (2014). A sphingolipid-dependent diffusion barrier confines ER stress to the yeast mother cell. eLife *3*, e01883.
14. Colacurcio, D.J., and Nixon, R.A. (2016). Disorders of lysosomal acidification-The emerging role of v-ATPase in aging and neurodegenerative disease. Ageing Res Rev *32*, 75-88.
15. David, D.C., Ollikainen, N., Trinidad, J.C., Cary, M.P., Burlingame, A.L., and Kenyon, C. (2010). Widespread Protein Aggregation as an Inherent Part of Aging in C. elegans. PLOS Biology *8*, e1000450.
16. Davidow, L.S., Goetsch, L., and Byers, B. (1980). Preferential Occurrence of Nonsister Spores in Two-Spored Asci of SACCHAROMYCES CEREVISIAE: Evidence for Regulation of Spore-Wall Formation by the Spindle Pole Body. Genetics *94*, 581-595.

17. De Virgilio, C., DeMarini, D.J., and Pringle, J.R. (1996). SPR28, a sixth member of the septin gene family in Saccharomyces cerevisiae that is expressed specifically in sporulating cells. Microbiology *142 (Pt 10)*, 2897-2905.

18. Denoth-Lippuner, A., Krzyzanowski, M.K., Stober, C., and Barral, Y. (2014). Role of SAGA in the asymmetric segregation of DNA circles during yeast ageing. eLife *3*.

19. Dultz, E., Zanin, E., Wurzenberger, C., Braun, M., Rabut, G., Sironi, L., and Ellenberg, J. (2008). Systematic kinetic analysis of mitotic dis- and reassembly of the nuclear pore in living cells. The Journal of cell biology *180*, 857-865.

20. Eastwood, M.D., Cheung, S.W., Lee, K.Y., Moffat, J., and Meneghini, M.D. (2012). Developmentally programmed nuclear destruction during yeast gametogenesis. Developmental cell *23*, 35-44.

21. Eastwood, M.D., and Meneghini, M.D. (2015). Developmental Coordination of Gamete Differentiation with Programmed Cell Death in Sporulating Yeast. Eukaryot Cell *14*, 858-867.

22. Eisenberg, A.R., Higdon, A., Keskin, A., Hodapp, S., Jovanovic, M., and Brar, G.A. (2018). Precise Post-translational Tuning Occurs for Most Protein Complex Components during Meiosis. Cell reports *25*, 3603-3617.e3602.

23. Erjavec, N., Larsson, L., Grantham, J., and Nystrom, T. (2007). Accelerated aging and failure to segregate damaged proteins in Sir2 mutants can be suppressed by overproducing the protein aggregation-remodeling factor Hsp104p. Genes Dev *21*, 2410-2421.

24. Fares, H., Goetsch, L., and Pringle, J.R. (1996). Identification of a developmentally regulated septin and involvement of the septins in spore formation in Saccharomyces cerevisiae. The Journal of cell biology *132*, 399-411.

25. Fawcett, D.W., and Chemes, H.E. (1979). Changes in distribution of nuclear pores during differentiation of the male germ cells. Tissue and Cell *11*, 147-162.

26. Fuchs, J., and Loidl, J. (2004). Behaviour of nucleolus organizing regions (NORs) and nucleoli during mitotic and meiotic divisions in budding yeast. Chromosome Res *12*, 427-438.

27. Glover, J.R., and Lindquist, S. (1998). Hsp104, Hsp70, and Hsp40: a novel chaperone system that rescues previously aggregated proteins. Cell *94*, 73-82.

28. Gorsich, S.W., and Shaw, J.M. (2004). Importance of mitochondrial dynamics during meiosis and sporulation. Molecular biology of the cell *15*, 4369-4381.

29. Goudeau, J., and Aguilaniu, H. (2010). Carbonylated proteins are eliminated during reproduction in C. elegans. Aging Cell *9*, 991-1003.

30. Henderson, K.A., Hughes, A.L., and Gottschling, D.E. (2014). Mother-daughter asymmetry of pH underlies aging and rejuvenation in yeast. eLife *3*, e03504.

31. Ho, H.C. (2010). Redistribution of nuclear pores during formation of the redundant nuclear envelope in mouse spermatids. J Anat *216*, 525-532.

32. Hochwagen, A., Tham, W.H., Brar, G.A., and Amon, A. (2005). The FK506 binding protein Fpr3 counteracts protein phosphatase 1 to maintain meiotic recombination checkpoint activity. Cell *122*, 861-873.

33. Hughes, A.L., and Gottschling, D.E. (2012). An early age increase in vacuolar pH limits mitochondrial function and lifespan in yeast. Nature *492*, 261-265.

34. Janke, C., Magiera, M.M., Rathfelder, N., Taxis, C., Reber, S., Maekawa, H., Moreno-Borchart, A., Doenges, G., Schwob, E., Schiebel, E.*, et al.* (2004). A versatile toolbox for PCR-based tagging of yeast genes: new fluorescent proteins, more markers and promoter substitution cassettes. Yeast *21*, 947-962.

35. Janssens, G.E., Meinema, A.C., Gonzalez, J., Wolters, J.C., Schmidt, A., Guryev, V., Bischoff, R., Wit, E.C., Veenhoff, L.M., and Heinemann, M. (2015). Protein biogenesis machinery is a driver of replicative aging in yeast. eLife *4*, e08527.

36. Kaeberlein, M. (2010). Lessons on longevity from budding yeast. Nature *464*, 513-519.

37. Kanki, T., and Klionsky, D.J. (2008). Mitophagy in yeast occurs through a selective mechanism. The Journal of biological chemistry *283*, 32386-32393.

38. King, M.C., Lusk, C.P., and Blobel, G. (2006). Karyopherin-mediated import of integral inner nuclear membrane proteins. Nature *442*, 1003-1007.

39. Knop, M., and Strasser, K. (2000). Role of the spindle pole body of yeast in mediating assembly of the prospore membrane during meiosis. Embo j *19*, 3657-3667.

40. Kremer, J.R., Mastronarde, D.N., and McIntosh, J.R. (1996). Computer visualization of three-dimensional image data using IMOD. Journal of structural biology *116*, 71-76.

41. Lam, C., Santore, E., Lavoie, E., Needleman, L., Fiacco, N., Kim, C., and Neiman, A.M. (2014). A visual screen of protein localization during sporulation identifies new components of prospore membrane-associated complexes in budding yeast. Eukaryot Cell *13*, 383-391.

42. Lee, W.C., Zabetakis, D., and Melese, T. (1992). NSR1 is required for pre-rRNA processing and for the proper maintenance of steady-state levels of ribosomal subunits. Mol Cell Biol *12*, 3865-3871.

43. Lewinska, A., Miedziak, B., Kulak, K., Molon, M., and Wnuk, M. (2014). Links between nucleolar activity, rDNA stability, aneuploidy and chronological aging in the yeast Saccharomyces cerevisiae. Biogerontology *15*, 289-316.

44. Li, P., Jin, H., Hoang, M.L., and Yu, H.G. (2011). Tracking chromosome dynamics in live yeast cells: coordinated movement of rDNA homologs and anaphase disassembly of the nucleolus during meiosis. Chromosome Res *19*, 1013-1026.

45. Longo, V.D., Shadel, G.S., Kaeberlein, M., and Kennedy, B. (2012). Replicative and chronological aging in Saccharomyces cerevisiae. Cell metabolism *16*, 18-31.

46. Longtine, M.S., McKenzie, A., 3rd, Demarini, D.J., Shah, N.G., Wach, A., Brachat, A., Philippsen, P., and Pringle, J.R. (1998). Additional modules for versatile and economical PCR-based gene deletion and modification in Saccharomyces cerevisiae. Yeast *14*, 953-961.

47. Lord, C.L., Timney, B.L., Rout, M.P., and Wente, S.R. (2015). Altering nuclear pore complex function impacts longevity and mitochondrial function in S. cerevisiae. The Journal of cell biology *208*, 729-744.

48. Markossian, S., Suresh, S., Osmani, A.H., and Osmani, S.A. (2015). Nup2 requires a highly divergent partner, NupA, to fulfill functions at nuclear pore complexes and the mitotic chromatin region. Molecular biology of the cell *26*, 605-621.

49. Matos, J., Lipp, J.J., Bogdanova, A., Guillot, S., Okaz, E., Junqueira, M., Shevchenko, A., and Zachariae, W. (2008). Dbf4-dependent CDC7 kinase links DNA replication to the segregation of homologous chromosomes in meiosis I. Cell *135*, 662-678.

50. McDonald, K., and Muller-Reichert, T. (2002). Cryomethods for thin section electron microscopy. Methods in enzymology *351*, 96-123.

51. McDonald, K.L. (2014). Out with the old and in with the new: rapid specimen preparation procedures for electron microscopy of sectioned biological material. Protoplasma *251*, 429-448.

52. McDonald, K.L., and Webb, R.I. (2011). Freeze substitution in 3 hours or less. Journal of microscopy *243*, 227-233.

53. Meinema, A.C., Laba, J.K., Hapsari, R.A., Otten, R., Mulder, F.A., Kralt, A., van den Bogaart, G., Lusk, C.P., Poolman, B., and Veenhoff, L.M. (2011). Long unfolded linkers facilitate membrane protein import through the nuclear pore complex. Science *333*, 90-93.

54. Meszaros, N., Cibulka, J., Mendiburo, M.J., Romanauska, A., Schneider, M., and Kohler, A. (2015). Nuclear pore basket proteins are tethered to the nuclear envelope and can regulate membrane curvature. Developmental cell *33*, 285-298.

55. Miyakawa, I., Aoi, H., Sando, N., and Kuroiwa, T. (1984). Fluorescence microscopic studies of mitochondrial nucleoids during meiosis and sporulation in the yeast, Saccharomyces cerevisiae. J Cell Sci *66*, 21-38.

56. Moens, P.B. (1971). Fine structure of ascospore development in the yeast Saccharomyces cerevisiae. Can J Microbiol *17*, 507-510.

57. Moens, P.B., and Rapport, E. (1971). Spindles, spindle plaques, and meiosis in the yeast Saccharomyces cerevisiae (Hansen). The Journal of cell biology *50*, 344-361.

58. Moreno-Borchart, A.C., Strasser, K., Finkbeiner, M.G., Shevchenko, A., Shevchenko, A., and Knop, M. (2001). Prospore membrane formation linked to the leading edge protein (LEP) coat assembly. Embo j *20*, 6946-6957.

59. Morlot, S., Song, J., Leger-Silvestre, I., Matifas, A., Gadal, O., and Charvin, G. (2018). Nucleolar stress causes the entry into replicative senescence in budding yeast. bioRxiv, 297093.

60. Mortimer, R.K., and Johnston, J.R. (1959). Life span of individual yeast cells. Nature *183*, 1751-1752.

61. Nakanishi, H., de los Santos, P., and Neiman, A.M. (2004). Positive and negative regulation of a SNARE protein by control of intracellular localization. Molecular biology of the cell *15*, 1802-1815.

62. Neiman, A.M. (1998). Prospore membrane formation defines a developmentally regulated branch of the secretory pathway in yeast. The Journal of cell biology *140*, 29-37.

63. Neiman, A.M. (2011). Sporulation in the budding yeast Saccharomyces cerevisiae. Genetics *189*, 737-765.

64. Okamoto, S., and Iino, T. (1981). Selective abortion of two nonsister nuclei in a developing ascus of the hfd-1 mutant in Saccharomyces cerevisiae. Genetics *99*, 197-209.

65. Ozsarac, N., Bhattacharyya, M., Dawes, I.W., and Clancy, M.J. (1995). The SPR3 gene encodes a sporulation-specific homologue of the yeast CDC3/10/11/12 family of bud neck microfilaments and is regulated by ABFI. Gene *164*, 157-162.

66. Rajoo, S., Vallotton, P., Onischenko, E., and Weis, K. (2018). Stoichiometry and compositional plasticity of the yeast nuclear pore complex revealed by quantitative fluorescence microscopy. Proc Natl Acad Sci U S A *115*, E3969-e3977.

67. Reynolds, E.S. (1963). The use of lead citrate at high pH as an electron-opaque stain in electron microscopy. The Journal of cell biology *17*, 208-212.

68. Saarikangas, J., Caudron, F., Prasad, R., Moreno, D.F., Bolognesi, A., Aldea, M., and Barral, Y. (2017). Compartmentalization of ER-Bound Chaperone Confines Protein Deposit Formation to the Aging Yeast Cell. Current biology : CB *27*, 773-783.

69. Sawyer, E.M., Joshi, P.R., Jorgensen, V., Yunus, J., Berchowitz, L.E., and Unal, E. (2019). Developmental regulation of an organelle tether coordinates mitochondrial remodeling in meiosis. The Journal of cell biology *218*, 559-579.

70. Schindelin, J., Arganda-Carreras, I., Frise, E., Kaynig, V., Longair, M., Pietzsch, T., Preibisch, S., Rueden, C., Saalfeld, S., Schmid, B.*, et al.* (2012). Fiji: an open-source platform for biological-image analysis. Nature methods *9*, 676-682.

71. Sheff, M.A., and Thorn, K.S. (2004). Optimized cassettes for fluorescent protein tagging in Saccharomyces cerevisiae. Yeast *21*, 661-670.

72. Sinclair, D.A., and Guarente, L. (1997). Extrachromosomal rDNA circles--a cause of aging in yeast. Cell *91*, 1033-1042.

73. Sinclair, D.A., Mills, K., and Guarente, L. (1997). Accelerated aging and nucleolar fragmentation in yeast sgs1 mutants. Science *277*, 1313-1316.

74. Smeal, T., Claus, J., Kennedy, B., Cole, F., and Guarente, L. (1996). Loss of transcriptional silencing causes sterility in old mother cells of S. cerevisiae. Cell *84*, 633-642.

75. Stevens, B. (1981). Mitochondrial structure. In Molecular Biology of the Yeast Saccharomyces, J.N. Strathern, E.W. Jones, and J.R. Broach, eds. (Cold Spring Harbor, NY: Cold Spring Harbor Laboratory Press), pp. 471-505.

76. Suda, Y., Nakanishi, H., Mathieson, E.M., and Neiman, A.M. (2007). Alternative modes of organellar segregation during sporulation in Saccharomyces cerevisiae. Eukaryot Cell *6*, 2009-2017.

77. Sun, N., Youle, R.J., and Finkel, T. (2016). The Mitochondrial Basis of Aging. Mol Cell *61*, 654-666.

78. Suresh, S., Markossian, S., Osmani, A.H., and Osmani, S.A. (2017). Mitotic nuclear pore complex segregation involves Nup2 in Aspergillus nidulans. The Journal of cell biology *216*, 2813-2826.

79. Taxis, C., Keller, P., Kavagiou, Z., Jensen, L.J., Colombelli, J., Bork, P., Stelzer, E.H., and Knop, M. (2005). Spore number control and breeding in Saccharomyces cerevisiae: a key role for a self-organizing system. The Journal of cell biology *171*, 627-640.

80. Tiku, V., Jain, C., Raz, Y., Nakamura, S., Heestand, B., Liu, W., Spath, M., Suchiman, H.E.D., Muller, R.U., Slagboom, P.E.*, et al.* (2017). Small nucleoli are a cellular hallmark of longevity. Nat Commun *8*, 16083.

81. Troyer, D., and Schwager, P. (1982). Evidence for nuclear membrane fluidity: Proacrosome migration and nuclear pore redistribution during grasshopper spermiogenesis. Cell Motility *2*, 355-367.

82. Unal, E., and Amon, A. (2011). Gamete formation resets the aging clock in yeast. Cold Spring Harbor symposia on quantitative biology *76*, 73-80.

83. Unal, E., Kinde, B., and Amon, A. (2011). Gametogenesis eliminates age-induced cellular damage and resets life span in yeast. Science *332*, 1554-1557.

84. Veatch, J.R., McMurray, M.A., Nelson, Z.W., and Gottschling, D.E. (2009). Mitochondrial dysfunction leads to nuclear genome instability via an iron-sulfur cluster defect. Cell *137*, 1247-1258.

85. Xu, L., Ajimura, M., Padmore, R., Klein, C., and Kleckner, N. (1995). NDT80, a meiosis-specific gene required for exit from pachytene in Saccharomyces cerevisiae. Mol Cell Biol *15*, 6572-6581.

TABLES

Table S1. Detailed genotypes of the strains used in this study.

Strain	Genotype
SK1 wild-type	*ho::LYS2 lys2 ura3 leu2::hisG his3::hisG trp1::hisG*
UB3810	*MAT**a** /MATalpha HTB1-mCherry::HISMX6/HTB1-mCherry::HISMX6 Nup53-eGFP:KanMX/Nup53-eGFP:KanMX*
UB8837	*MAT**a** /MATalpha GAL-NDT80::TRP1/GAL-NDT80::TRP1 ura3::pGPD1-GAL4(848).ER::URA3/ura3::pGPD1-GAL4(848).ER::URA3 Nup170-3xDendra::HISMX/Nup170-3xDendra::HISMX*
UB8839	*MAT**a** /MATalpha GAL-NDT80::TRP1/GAL-NDT80::TRP1 ura3::pGPD1-GAL4(848).ER::URA3/ura3::pGPD1-GAL4(848).ER::URA3 Nup49-3xDendra::HISMX/Nup49-3xDendra-HISMX*
UB9724	*MAT**a** /MATalpha HTB1-mCherry::HISMX6/HTB1-mCherry::HISMX6 Hsp104-eGFP::KanMX/Hsp104-eGFP::KanMX flo8::KanMX6/ flo8::KanMX6*
UB11513	*MAT**a** /MATalpha HTB1-mCherry::HISMX6/HTB1-mCherry::HISMX6 Nup170-GFP::KanMX/Nup170-GFP::KanMX*
UB11821	*MAT**a** /MATalpha Hsp104-mCherry::NatMX/Hsp104-mCherry::NatMX leu2::pATG8-link-yeGFP-SPO20(51-91)::LEU2/leu2::pATG8-link-yeGFP-SPO20(51-91)::LEU2 flo8::KanMX6/flo8::KanMX6*
UB12163	*MAT**a** /MATalpha flo8::KanMX6/flo8::KanMX6 Hsp104-mCherry::NatMX/Hsp104-mCherry::NatMX his3::VPH1-eGFP::HIS3/ his3::VPH1-eGFP::HIS3*
UB12342	*MAT**a** /MATalpha leu2::pATG8-link-yeGFP-SPO20(51-91)::LEU2/ leu2::pATG8-link-yeGFP-SPO20(51-91)::LEU2 Nup49-mCherry::KanMX/ Nup49-mCherry::KanMX*
UB12414	*MAT**a** /MATalpha Ady3::HygB/Ady3::HygB HTB1-mCherry::HISMX6/ HTB1-mCherry::HISMX6 Nup170-GFP::KanMX/Nup170-GFP::KanMX*
UB12434	*MAT**a** /MATalpha leu2::pATG8-link-yeGFP-SPO20(51-91)::LEU2/ leu2::pATG8-link-yeGFP-SPO20(51-91)::LEU2 HTB1-mCherry::HISMX6/HTB1-mCherry::HISMX6*
UB12436	*MAT**a** /MATalpha Don1-GFP::KanMX/Don1-GFP::KanMX Nup49-mCherry::KanMX/Nup49-mCherry::KanMX*
UB12438	*MAT**a** /MATalpha Don1-GFP::KanMX/Don1-GFP::KanMX HTB1-mCherry::HISMX6/HTB1-mCherry::HISMX6*
UB12461	*MAT**a** /MATalpha Don1::HygB/Don1::HygB Nup170-GFP::KanMX/Nup170-GFP::KanMX HTB1-mCherry::HISMX6/HTB1-mCherry::HISMX6*

UB12463	*MAT**a** /MATalpha Irc10::HygB/Irc10::HygB Nup170-GFP::KanMX/Nup170-GFP::KanMX HTB1-mCherry::HISMX6/HTB1-mCherry::HISMX6*
UB12465	*MAT**a** /MATalpha ady3::HygB/ady3::HygB irc10::HygB/irc10::HygB Nup170-GFP::KanMX/Nup170-GFP::KanMX HTB1-mCherry::HISMX6/ HTB1-mCherry::HISMX6*
UB12932	*MAT**a** /MATalpha leu2::pARO10-eGFP-h2NLS-L-TM::LEU2/leu2:: pARO10-eGFP-h2NLS-L-TM::LEU2 Nup49-mCherry::KanMX/ Nup49-mCherry::KanMX*
UB12975	*MAT**a** /MATalpha Nup170-GFP::KanMX/ Nup170-GFP::KanMX Hsp104-mCherry::NatMX/Hsp104-mCherry::NatMX flo8::KanMX6/flo8::KanMX6*
UB13299	*MAT**a** /MATalpha Nsr1-GFP::KanMX/ Nsr1-GFP::KanMX Hsp104-mCherry::NatMX/Hsp104-mCherry::NatMX flo8::KanMX6/flo8::KanMX6*
UB13373	*MAT**a** /MATalpha ssp1::KanMX/ ssp1::KanMX Nup170-GFP::KanMX/Nup170-GFP::KanMX HTB1-mCherry::HISMX6/HTB1-mCherry::HISMX6*
UB13377	*MAT**a** /MATalpha spo21::HygB/spo21::HygB Nup170-GFP::KanMX/Nup170-GFP::KanMX HTB1-mCherry::HISMX6/HTB1-mCherry::HISMX6*
UB13473	*MAT**a** /MATalpha ssp1::KanMX/ ssp1::KanMX leu2::pATG8-link-yeGFP-SPO20(51-91)::LEU2/ leu2::pATG8-link-yeGFP-SPO20(51-91)::LEU2 Nup49-mCherry::KanMX/ Nup49-mCherry::KanMX*
UB13475	*MAT**a** /MATalpha ssp1::KanMX/ ssp1::KanMX leu2::pATG8-link-yeGFP-SPO20(51-91)::LEU2/ leu2::pATG8-link-yeGFP-SPO20(51-91)::LEU2 HTB1-mCherry::HISMX6/HTB1-mCherry::HISMX6*
UB13497	*MAT**a** /MATalpha Nup84-GFP::KanMX/ Nup84-GFP::KanMX HTB1-mCherry::HISMX6/HTB1-mCherry::HISMX6*
UB13499	*MAT**a** /MATalpha Nup120-GFP::KanMX/Nup120-GFP::KanMX HTB1-mCherry::HISMX6/HTB1-mCherry::HISMX6*
UB13503	*MAT**a** /MATalpha Pom34-GFP::KanMX/Pom34-GFP::KanMX HTB1-mCherry::HISMX6/HTB1-mCherry::HISMX6*
UB13505	*MAT**a** /MATalpha Nup188-GFP::KanMX/Nup188-GFP::KanMX HTB1-mCherry::HISMX6/HTB1-mCherry::HISMX6*
UB13509	*MAT**a** /MATalpha Nup49-GFP::KanMX/Nup49::KanMX HTB1-mCherry::HISMX6/HTB1-mCherry::HISMX6*
UB13568	*MAT**a** /MATalpha spo21::HygB/spo21::HygB Hsp104-mCherry::NatMX/ Hsp104-mCherry::NatMX Nup170-GFP::KanMX/Nup170-GFP::KanMX flo8::KanMX6/flo8::KanMX6*
UB13583	*MAT**a** /MATalpha ady3::HygB/ady3::HygB Irc10::HygB/Irc10::HygB leu2::pATG8-link-yeGFP-SPO20(51-91)::LEU2/ leu2::pATG8-link-yeGFP-SPO20(51-91)::LEU2 Nup49-mCherry::KanMX/ Nup49-mCherry::KanMX*
UB13585	*MAT**a** /MATalpha ady3::HygB/ady3::HygB Irc10::HygB/Irc10::HygB leu2::pATG8-link-yeGFP-SPO20(51-91)::LEU2/ leu2::pATG8-link-yeGFP-SPO20(51-91)::LEU2 HTB1-mCherry::HISMX6/HTB1-mCherry::HISMX6*

UB14391	*MATa /MATalpha Heh1-3xeGFP::KanMX/Heh1-3xeGFP::KanMX Nup49-mCherry::KanMX/ Nup49-mCherry::KanMX*
UB14393	*MATa /MATalpha Heh1-3xeGFP::KanMX/Heh1-3xeGFP::KanMX HTB1-mCherry::HISMX6/ HTB1-mCherry::HISMX6*
UB14418	*MATa /MATalpha HTB1-mCherry::HISMX6/HTB1-mCherry::HISMX6 Hsp104-eGFP::KanMX/Hsp104-eGFP::KanMX flo8::KanMX6/ flo8::KanMX6 spo21::HygB/spo21::HygB*
UB14419	*MATa /MATalpha HTB1-mCherry::HISMX6/HTB1-mCherry::HISMX6 Nsr1-GFP::KanMX/ Nsr1-GFP::KanMX spo21::HygB/spo21::HygB*
UB14425	*MATa /MATalpha Nsr1-GFP::KanMX/ Nsr1-GFP::KanMX Nup49-mCherry::KanMX/ Nup49-mCherry::KanMX spo21::HygB/spo21::HygB*
UB14646	*MATa /MATalpha Nup60-GFP::KanMX/ Nup60-GFP::KanMX HTB1-mCherry::HISMX6/HTB1-mCherry::HISMX6*
UB14650	*MATa /MATalpha Nup159-GFP::KanMX/ Nup159-GFP::KanMX HTB1-mCherry::HISMX6/HTB1-mCherry::HISMX6*
UB14652	*MATa /MATalpha Nup82-GFP::KanMX/ Nup82-GFP::KanMX HTB1-mCherry::HISMX6/HTB1-mCherry::HISMX6*
UB14654	*MATa /MATalpha Nup57-GFP::KanMX/Nup57-GFP::KanMX HTB1-mCherry::HISMX6/HTB1-mCherry::HISMX6*
UB15118	*MATa /MATalpha Nsr1-GFP::KanMX/ Nsr1-GFP::KanMX HTB1-mCherry::HISMX6/HTB1-mCherry::HISMX6*
UB15301	*MATa /MATalpha Ndc1-GFP::KanMX/ Ndc1-GFP::KanMX HTB1-mCherry::HISMX6/HTB1-mCherry::HISMX6*
UB15303	*MATa /MATalpha Nup1-GFP::KanMX/ Nup1-GFP::KanMX HTB1-mCherry::HISMX6/HTB1-mCherry::HISMX6*
UB15305	*MATa /MATalpha Nup2-GFP::KanMX/ Nup2-GFP::KanMX HTB1-mCherry::HISMX6/HTB1-mCherry::HISMX6*
UB15307	*MATa /MATalpha spr3::HygB/ spr3::HygB Nup170-GFP::KanMX/ Nup170-GFP::KanMX HTB1-mCherry::HISMX6/ HTB1-mCherry::HISMX6*
UB15426	*MATa /MATalpha spr28::HygB/ spr28::HygB Nup170-GFP::KanMX/ Nup170-GFP::KanMX HTB1-mCherry::HISMX6/ HTB1-mCherry::HISMX6*
UB15428	*MATa /MATalpha spr3::HygB/ spr3::HygB spr28::HygB/ spr28::HygB Nup170-GFP::KanMX/ Nup170-GFP::KanMX HTB1-mCherry::HISMX6/ HTB1-mCherry::HISMX6*
UB15672	*MATa /MATalpha Nup2-GFP::KanMX/ Nup2-GFP::KanMX Nup49-mCherry::KanMX/ Nup49-mCherry::KanMX*
UB15890	*MATa /MATalpha Nup170-GFP::KanMX/Nup170-GFP::KanMX Vph1-mCherry::HisMX/Vph1-mCherry::HisMX*
UB16708	*MATa /MATalpha Nsr1-GFP::KanMX/ Nsr1-GFP::KanMX Nup49-mCherry::KanMX/ Nup49-mCherry::KanMX flo8/flo8*

UB16710	*MAT**a** /MATalpha Nsr1-GFP::KanMX/ Nsr1-GFP::KanMX leu2::pATG8-link-mKate-SPO20(51-91)::LEU2/leu2::pATG8-link-mKate-SPO20(51-91)::LEU2 flo8/flo8*
UB16712	*MAT**a** /MATalpha Nsr1-GFP::KanMX/ Nsr1-GFP::KanMX HTB1-mCherry::HISMX6/ HTB1-mCherry::HISMX6 flo8/flo8*
UB17338	*MAT**a** /MATalpha Hta1-mApple::HIS5/ Hta1-mApple::HIS5 rDNA-5xtetO/rDNA pREC8-TetR-GFP::LEU2/ pREC8-TetR-GFP::LEU2 flo8/flo8 * Derived from HY2545*
UB17509	*MAT**a** /MATalpha Hta1-mApple::HIS5/ Hta1-mApple::HIS5 pREC8-TetR-GFP::LEU2/ pREC8-TetR-GFP::LEU2 flo8/flo8 * Derived from HY2545*
UB17532	*MAT**a** /MATalpha Nup49-mcherry::KanMX/ Nup49-mcherry::KanMX Hta1-mApple::His5 rDNA-5xtetO/rDNA pREC8-TetR-GFP::LEU2/ pREC8-TetR-GFP::LEU2 flo8/flo8 * Derived from HY2545*
UB19927	*MAT**a** /MATalpha HTB1-mCherry::HISMX6/HTB1-mCherry::HISMX6 Nup170-GFP::KanMX/Nup170-GFP::KanMX ndt80::LEU2/ndt80::LEU2*
UB19229	*MAT**a** /MATalpha Nup84-GFP::KanMX/ Nup84-GFP::KanMX HTB1-mCherry::HISMX6/HTB1-mCherry::HISMX6 ndt80::LEU2/ndt80::LEU2*
UB19752	*MAT**a** /MATalpha Hsp104-mCherry::NatMX/Hsp104-mCherry::NatMX leu2::pATG8-link-yeGFP-SPO20(51-91)::LEU2/leu2::pATG8-link-yeGFP-SPO20(51-91)::LEU2 flo8::KanMX6/flo8::KanMX6 spr3::HygB/ spr3::HygB*
UB19754	*MAT**a** /MATalpha Hsp104-mCherry::NatMX/Hsp104-mCherry::NatMX leu2::pATG8-link-yeGFP-SPO20(51-91)::LEU2/leu2::pATG8-link-yeGFP-SPO20(51-91)::LEU2 flo8::KanMX6/flo8::KanMX6 spr28::HygB/ spr28::HygB*
UB19756	*MAT**a** /MATalpha Hsp104-mCherry::NatMX/Hsp104-mCherry::NatMX leu2::pATG8-link-yeGFP-SPO20(51-91)::LEU2/leu2::pATG8-link-yeGFP-SPO20(51-91)::LEU2 flo8::KanMX6/flo8::KanMX6 don1::HygB/don1::HygB*
UB19758	*MAT**a** /MATalpha Hsp104-mCherry::NatMX/Hsp104-mCherry::NatMX leu2::pATG8-link-yeGFP-SPO20(51-91)::LEU2/leu2::pATG8-link-yeGFP-SPO20(51-91)::LEU2 flo8::KanMX6/flo8::KanMX6 ady3::HygB/ady3::HygB*
UB19760	*MAT**a** /MATalpha Hsp104-mCherry::NatMX/Hsp104-mCherry::NatMX leu2::pATG8-link-yeGFP-SPO20(51-91)::LEU2/leu2::pATG8-link-yeGFP-SPO20(51-91)::LEU2 flo8::KanMX6/flo8::KanMX6 spr3::HygB/ spr3::HygB spr28::HygB/ spr28::HygB*
UB19762	*MAT**a** /MATalpha Hsp104-mCherry::NatMX/Hsp104-mCherry::NatMX leu2::pATG8-link-yeGFP-SPO20(51-91)::LEU2/leu2::pATG8-link-yeGFP-SPO20(51-91)::LEU2 flo8::KanMX6/flo8::KanMX6 irc10::HygB/irc10::HygB*
HY2545	*ura3* his3Δ200 leu2-k lys2 ho::LYS2 *rDNA-5xtetO/ ura3* his3Δ200 lys2 ho::LYS2 *rDNA-5xtetO Hta1-mApple::HIS5 pREC8-TetR-GFP::LEU2*

Table S2. Primers used for strain construction in this study.

Construct name	Forward primer	Reverse primer
HEH1-3xeGFP	GGAACTCAATGAACCTAAGGATTC CGCTGAAAACAAAATA**cggatccccg ggttaattaa**	TTTGAGAAGAGAAAACTACGTTTGAG TTTCATTTTGTGGG**GAATTCGAGCTC GTTTAAAC**
NUP53-eGFP	AAATAGATTGAATAATTGGTTATTT GGATGGAATGATTTG**ggtgacggtgc tggttta**	AATCGCACCAAAGCACTACATTTGGG GGTAAGGTTTTTCA**tcgatgaattcgagc**
NUP84-GFP	GTATCTGGATCTCGTTGCTCGCAC AGCAACCCTTTCGAAT**CGGATCCC CGGGTTAATTAA**	TTACTTAAAATATAAACTTATTCTGCA ATACATTAATTGA**GAATTCGAGCTCG TTTAAAC**
NUP120-GFP	GGTTACTTTAACTGATTTAAGAGAT GAGTTACGAGGTCTA**CGGATCCCC GGGTTAATTAA**	ATTTTTTAAATGAAGTATTAATTTACA GTTTATATATTCA**GAATTCGAGCTCGT TTAAAC**
NUP170-GFP	GAACAGCGGCAATAATTTGGGGAT TTGTTTCTACAAAGAA**CGGATCCC CGGGTTAATTAA**	ACGTACATTACCCTGCTATCTATATGT CGAACATGAATTT**GAATTCGAGCTCG TTTAAAC**
POM34-GFP	TGCATATATGATGAACTCACAGTC CCCAAGGGGTAAAATA**CGGATCCC CGGGTTAATTAA**	TATATAGCTATGGAAAGTATTAAATG TTTTTTTGCTGTTT**GAATTCGAGCTCG TTTAAAC**
NUP188-GFP	AGACATTAAAGCATTACAAGATTC ACTATTCAAGGACGTT**CGGATCCC CGGGTTAATTAA**	ATTATTATATTATGTAGCTTTACATAA CTTACAAAATAAG**GAATTCGAGCTCG TTTAAAC**
NDC1-GFP	GTTTCTAGAAGTGTACGCCTCAGG CAACCCTAATGCTACG**CGGATCCC CGGGTTAATTAA**	ACATGAAATGGGAGGAGGGGTGCTC CTCGGTTGAATTGTA**GAATTCGAGCT CGTTTAAAC**
HSP104-mCherry	CGATAATGAGGACAGTATGGAAAT TGATGATGACCTAGAT**CGGATCCC CGGGTTAATTAA**	ATTCTTGTTCGAAAGTTTTTAAAAATC ACACTATATTAAA**GAATTCGAGCTCG TTTAAAC**
ssp1Δ	GGCGACACAAAATCATGAAG	TGATGTTTATGTATAGATCTCTCGA
NSR1-GFP	AAATACCGCTTCTTTCGCTGGTTCA AAGAAAACATTTGAT**CGGATCCCC GGGTTAATTAA**	AAGAGAAAAAATTGAAATTGAAATTC ATTTCATTTTCTCA**GAATTCGAGCTCG TTTAAAC**
don1Δ	TTTGGCTGGTATTTAAACACAAGT AAGAGAAGCATCAAAC**CGGATCCC CGGGTTAATTAA**	GCACTTTGCCGAAAGAGTTAATAAAC ATTACCGCTATACA**GAATTCGAGCTC GTTTAAAC**
DON1-GFP	AAAGCAGGTTCATCCATCTAGACA AGAATTAAGTTTTACG**CGGATCCC CGGGTTAATTAA**	GCACTTTGCCGAAAGAGTTAATAAAC ATTACCGCTATACA**GAATTCGAGCTC GTTTAAAC**
ady3Δ	TTTTGAATGGGATAGTTGAATACA ACAAACTTCTCCGAAT**CGGATCCC CGGGTTAATTAA**	ACACCATTGAATATATTAGTTCTAAAT AAAAAAAAAAAAG**GAATTCGAGCTC GTTTAAAC**

irc10Δ	AGTCTGCGGTATAATCACCTGGCC TAGTGCTTTTTCAATC**CGGATCCCC GGGTTAATTAA**	CTATATGTCAAGGGTGTCCCAAAATA AAAACTAACAGTAC**GAATTCGAGCTC GTTTAAAC**
NUP60-GFP	TGAAAATAAAGTTGAGGCTTTCAA GTCCCTATATACCTTT**CGGATCCCC GGGTTAATTAA**	GGGCTATACGGTAATTATGTCACGGC TAAAATTTTCATTA**GAATTCGAGCTC GTTTAAAC**
NUP159-GFP	GCAAATTGGTGATTTCTTCAAAAAT TTGAACATGGCAAAA**CGGATCCCC GGGTTAATTAA**	TTATTAACGGCACTAACAACGTACAT ATAGCTAAATATCA**GAATTCGAGCTC GTTTAAAC**
NUP82-GFP	ATTGTTACAAGTTTCTCAGGAATTT ACTACTAAAACTCAA**CGGATCCCC GGGTTAATTAA**	TAGCGTACATATATGATAGCAGACTA TGCAAGTCGCTTAC**GAATTCGAGCTC GTTTAAAC**
NUP57-GFP	GAAAGATGCTGCAATTGTAAAAAA ATATAAAAATAAAACG**CGGATCCC CGGGTTAATTAA**	CGATCTTTATACAATTCAGTCATTGAT TTAAGTAACCTGA**GAATTCGAGCTCG TTTAAAC**
NUP1-GFP	GGCGAACAGAAAGATTGCAAGAA TGAGGCACTCTAAAAGG**CGGATCC CCGGGTTAATTAA**	TTCAGAAAAGCAACACAATACCTAAT TACATAACCGATAT**GAATTCGAGCTC GTTTAAAC**
NUP2-GFP	ATTTACGAAAGCTATTGAAGATGC TAAAAAAGAAATGAAA**CGGATCCC CGGGTTAATTAA**	AGGGTTCTATTCTATTTAAAATTGTTA ACTGTATTTACTC**GAATTCGAGCTCGT TTAAAC**
spr3Δ	TAAAAACCTAAAATTCCTTTTGCGT CATTGAATTTTTATT**CGGATCCCCG GGTTAATTAA**	TTGCGCGAAATTATTGGCTTTTTTTTT TTTTTAATTAATA**GAATTCGAGCTCGT TTAAAC**
spr28Δ	AAAGAGCTACTATACGTACATAAA GTCAGTAAATAATCAA**CGGATCCC CGGGTTAATTAA**	ATTTCATATGTATCTAACGCTAACAAG GCCGTATATTTAT**GAATTCGAGCTCG TTTAAAC**
CFI1-GFP	TGGTGGATTTGCATCATTAATAAA AGATTTCAAGAAAAAA**CGGATCCC CGGGTTAATTAA**	TAGCTTTCTGTGACGTGTATTCTACTG AGACTTTCTGGTA**GAATTCGAGCTCG TTTAAAC**
VPH1-GFP	GGAAGTCGCTGTTGCTAGTGCAAG CTCTTCCGCTTCAAGC**CGTACGCTG CAGGTCGAC**	AGTACTTAAATGTTTCGCTTTTTTTAA AAGTCCTCAAAAT**ATCGATGAATTCG AGCTCG**
NUP49-GFP *NUP49-mCherry*	GAATCGCCGTGTTACATCAA AAAACGAAAACACTGGCAT CATTGAGCATA**cggatccccgg gttaattaa**	AGACATTTGTACTTGTTATACG CACTATATAAACTTTCAGGGC GATTTAC**gaattcgagctcgtttaaac**

Table S3. Plasmids used for strain construction in this study.

Plasmid Name	Description
pUB4	pFA6a-GFP(S65T)-KanMX6
pUB72	pFA6a-mCherry-KanMX6
pUB73	pFA6a-mCherry-NatMX6
pUB76	pFA6a-link-yeGFP-Kan
pUB217	pFA6a-HphNT1
pUB691	pNH603-HIS3-VPH1-eGFP
pUB949	pLC605-pATG8-link-yeGFP-SPO20(51-91)
pUB985	pFA6-3xeGFP-KanMX6
pUB1104	pLC605-pATG8-link-mKate-SPO20(51-91)
pUB1196	pLC605-pARO10-eGFP-h2NLS-L-TM
pUB1197	pYM28-mCherry-His3MX6

Table S4. Imaging conditions used.

Figure	RFP	GFP	BFP/DAPI	POL	Sectioning
3B-3G, 3 – S1A-B, 3 – S2, 3 – S3, 3 – S4, 3 – S5, 3 – S6A-B, 6 – S1A, 8A, 8 – S1A-B, 8 – S2A-B	10%T, 0.025s EX: 575/25 EM: 632/60	10%T, 0.025s EX: 475/28 EM: 523/36	N/A	32%T, 0.1s	1 µm, 8 sections
1B-1C, 1 – S1-S2, 2A-2B, 2E, 3H, 4A-4C, 5B-5C, 5 – S1A-B, 6C-6D***, 6 – S1B, 6 – S2A-S2B, , 6 – S4, 7A, 7C, 8 – S1C, 8 – S2C, 9A-B, 9D-E, 9 – S1A-B, 9 – S2A-B	32%T, 0.025s EX: 575/25 EM: 632/60	10%T, 0.025s EX: 475/28 EM: 523/36	N/A	32%T, 0.1s	1 µm, 8 sections
5A-B, 6A*, 6B, 8C-D	100%T, 0.1s EX: 575/25 EM: 632/60	100%T, 0.1s EX: 475/28 EM: 523/36	100%T, 0.01s EX: 390/18 EM: 435/48	32%T, 0.1s	0.2 µm, 40 sections
8F	100%T, 0.1s EX: 575/25 EM: 632/60	100%T, 0.1s EX: 475/28 EM: 523/36	100%T, 0.01s EX: 390/18 EM: 435/48	32%T, 0.1s	1 µm, 8 sections
4 – S1-S2**	100%T, 0.1s EX: 575/25 EM: 632/60	100%T, 0.1s EX: 475/28 EM: 523/36	100%T, 0.1s EX: 390/18 EM: 435/48	32%T, 0.1s	0.2 µm, 50 sections

*In 5A, the early and late meiosis II cells were acquired with 0.2 µm over 30 sections.
**In 4 – S1 and 4 – S2, pre-meiosis cells were acquired with 0.3 µm over 33 sections.
*** In 6C-6D, POL images were not acquired.

Table S5. Meiotic septin and leading edge complex genes are not required for nuclear pore complex or protein aggregate sequestration.

Function	Gene	NPC Strain (Nup170-GFP)	Protein Aggregate strain (Hsp104-GFP)
Leading edge	*ady3Δ*	UB12414	UB19758
	don1Δ	UB12461	UB19756
	irc10Δ	UB12463	UB19762
Meiotic septins	*spr3Δ*	UB15307	UB19752
	spr28Δ	UB15426	UB19754
	spr3Δspr28Δ	UB15428	UB19760

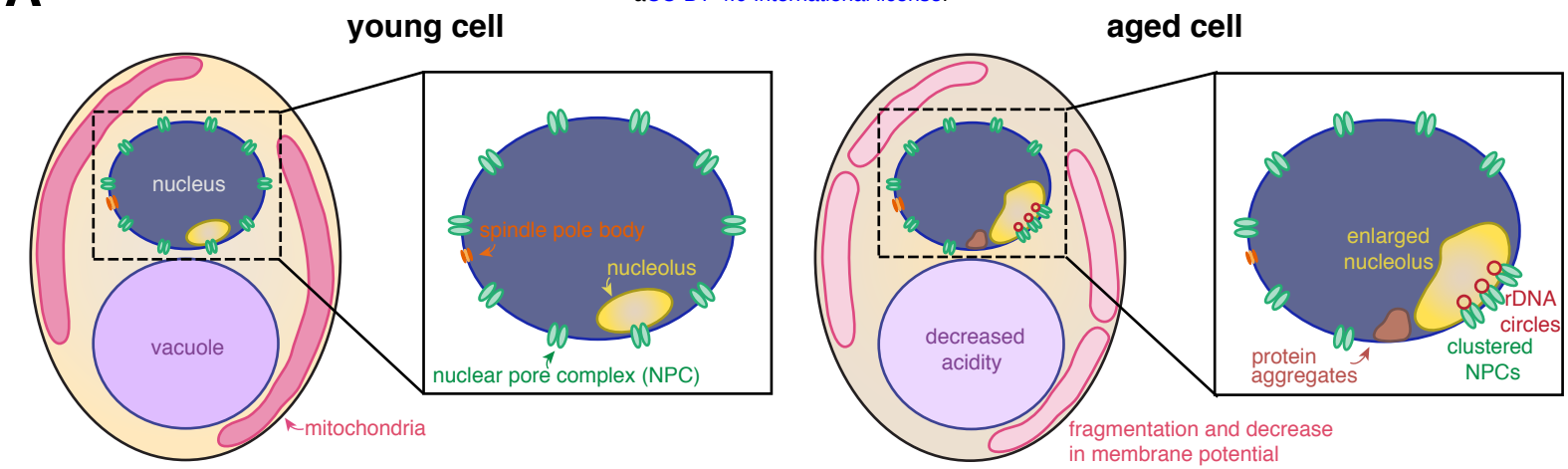

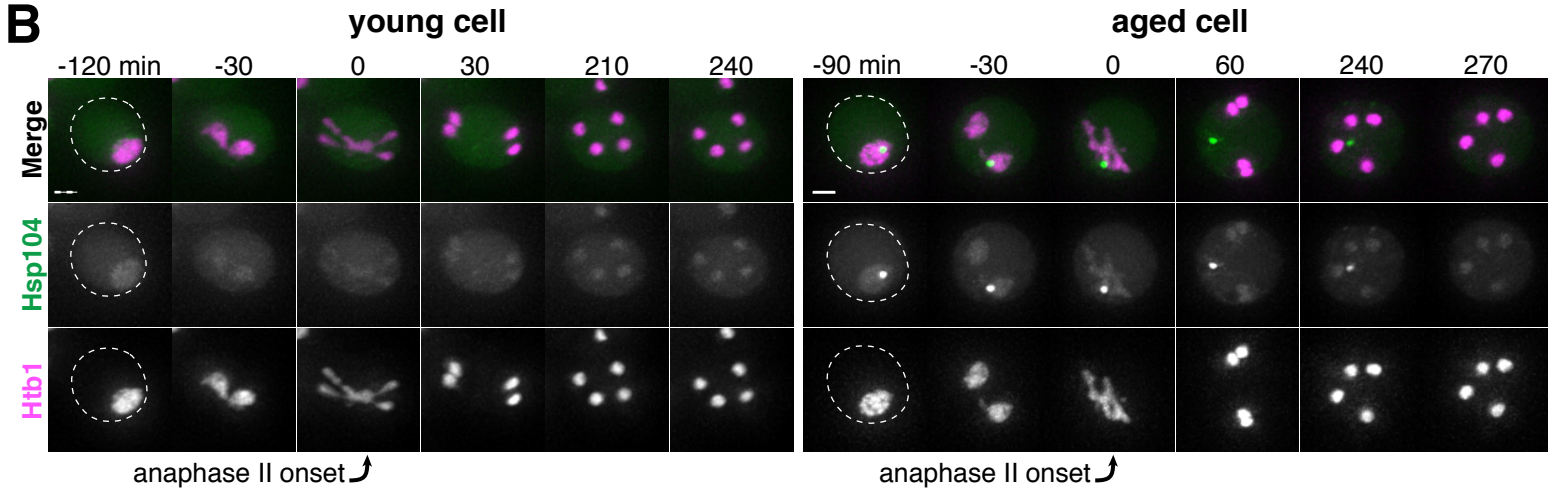

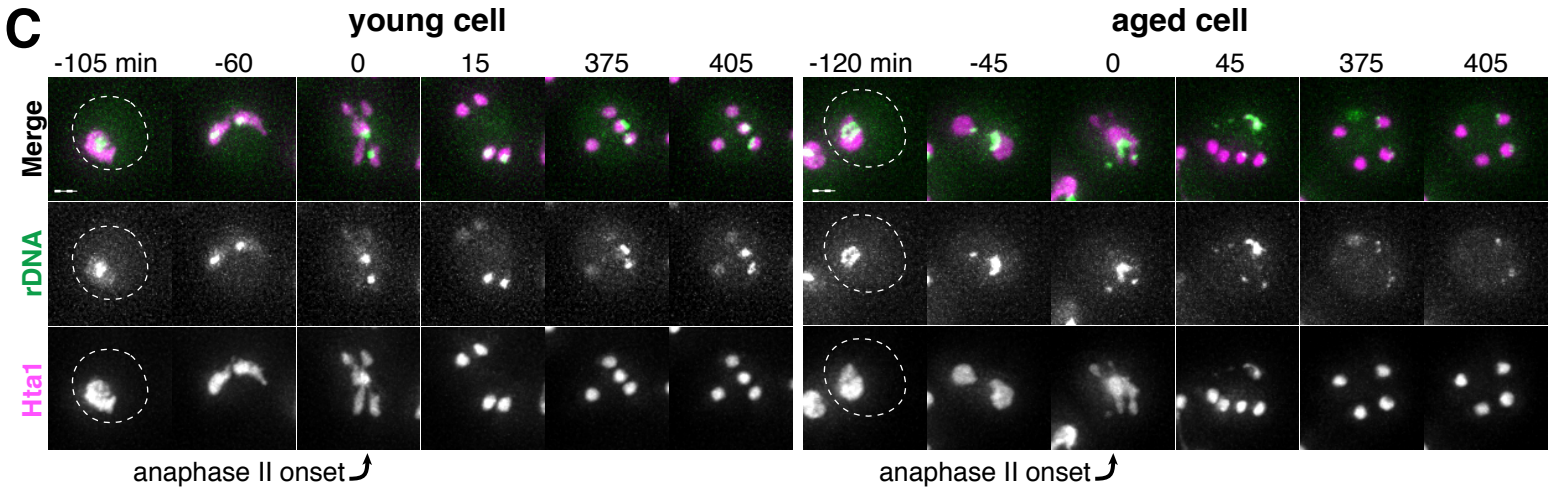

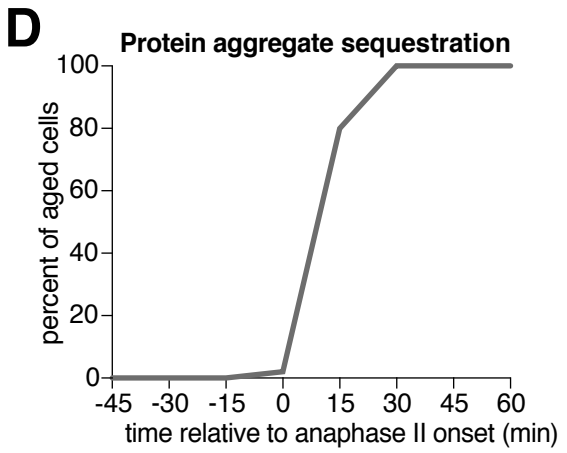

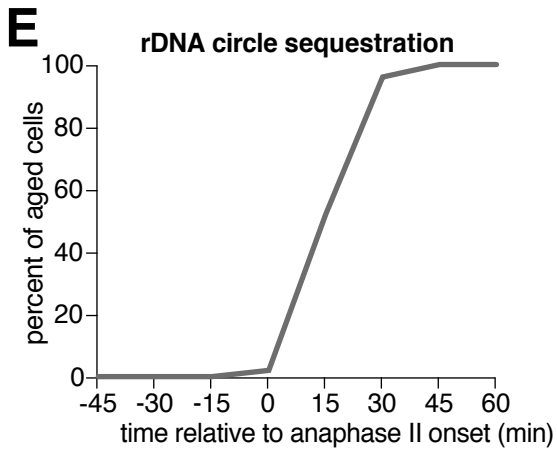

King and Goodman et al. Figure 1

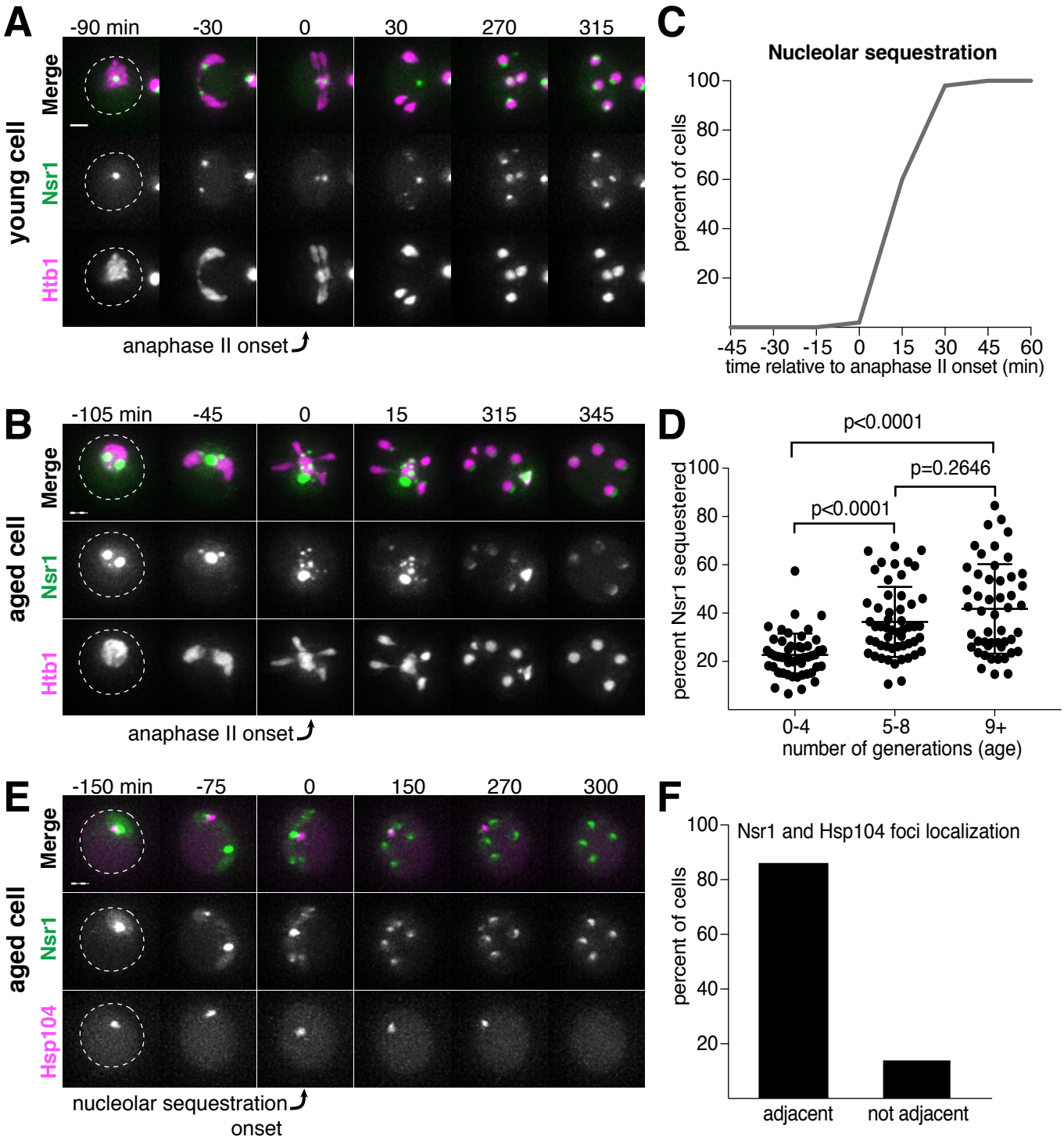

King and Goodman et al. Figure 2

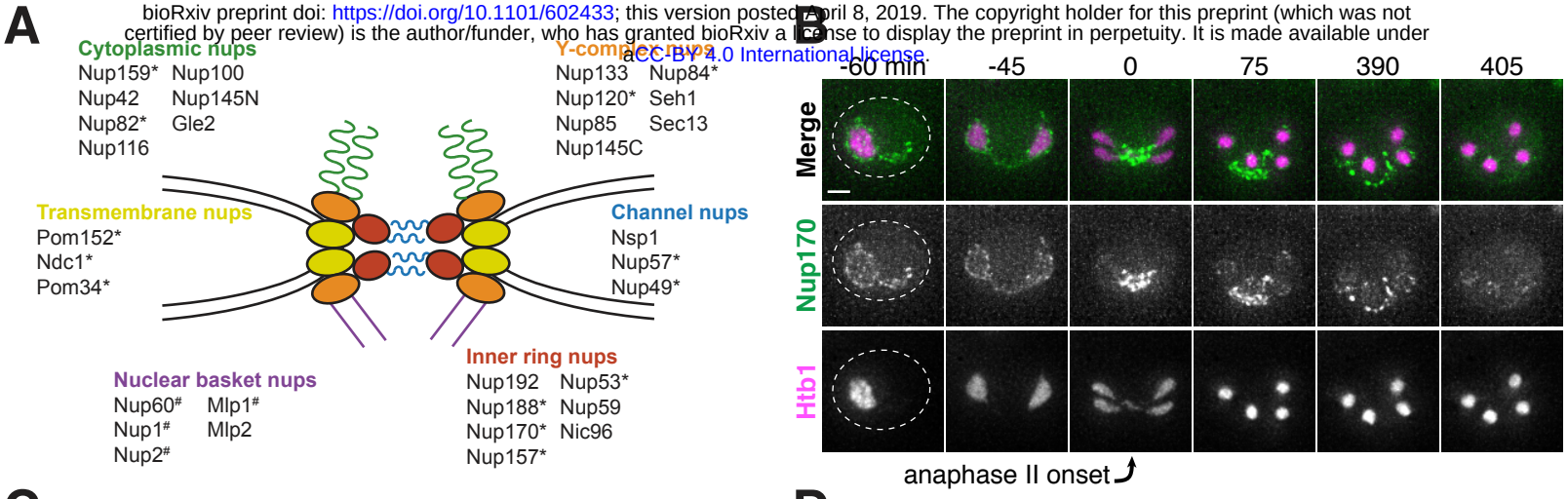

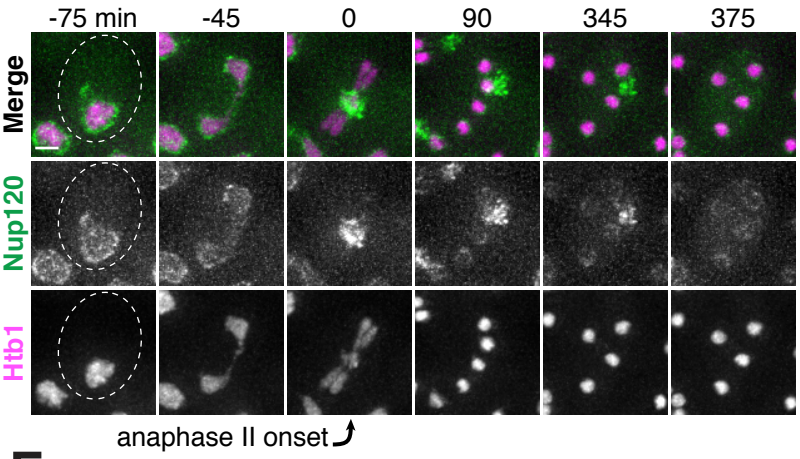

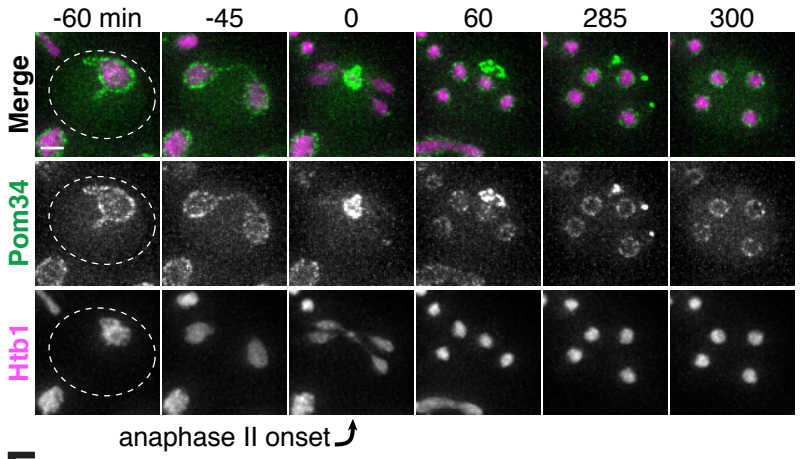

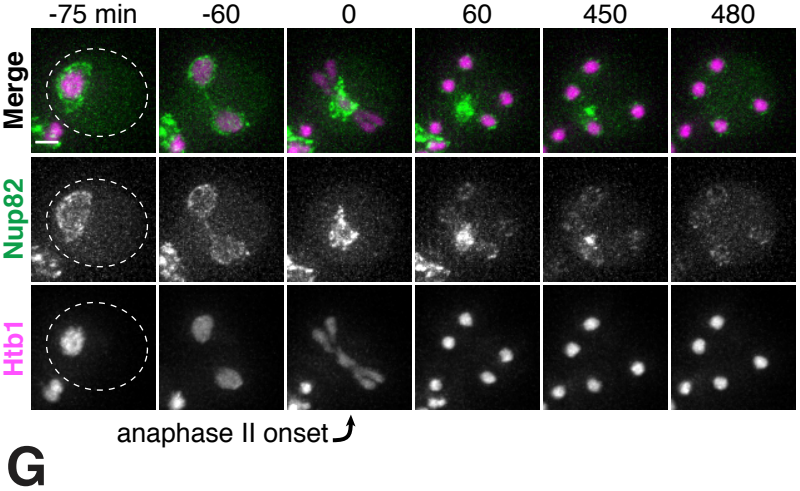

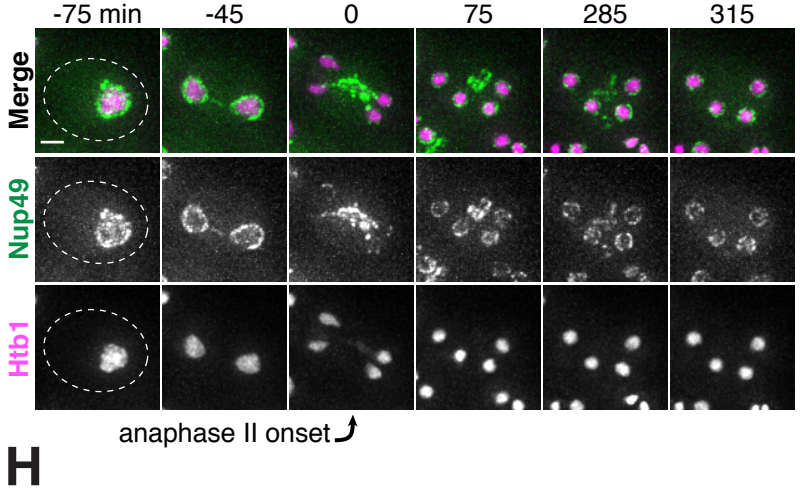

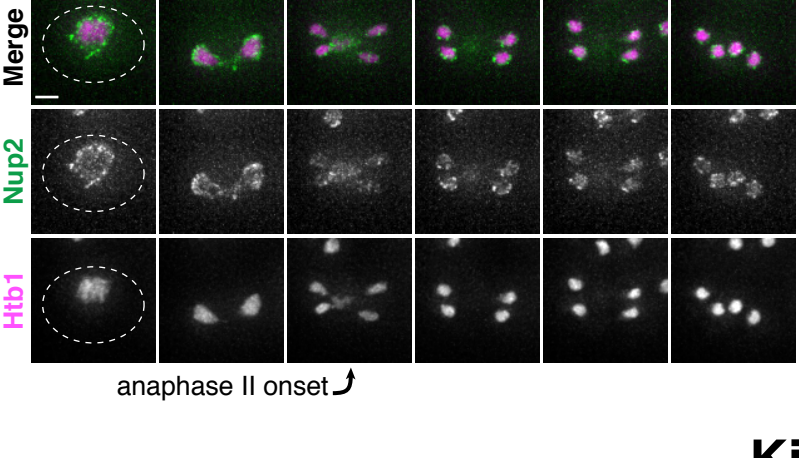

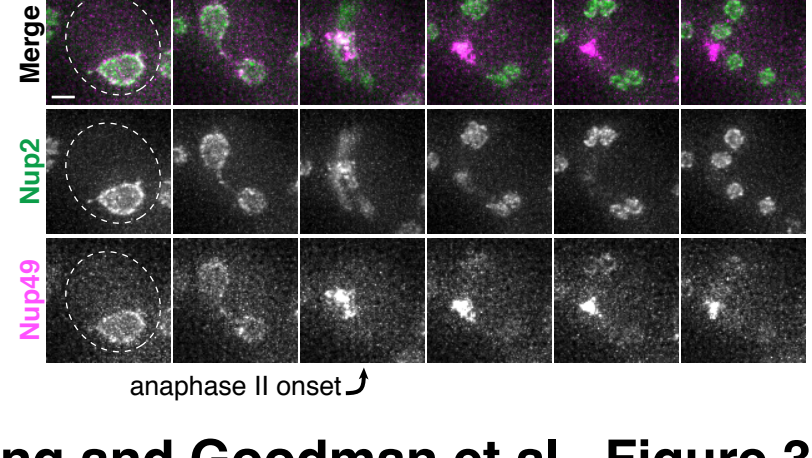

King and Goodman et al. Figure 3

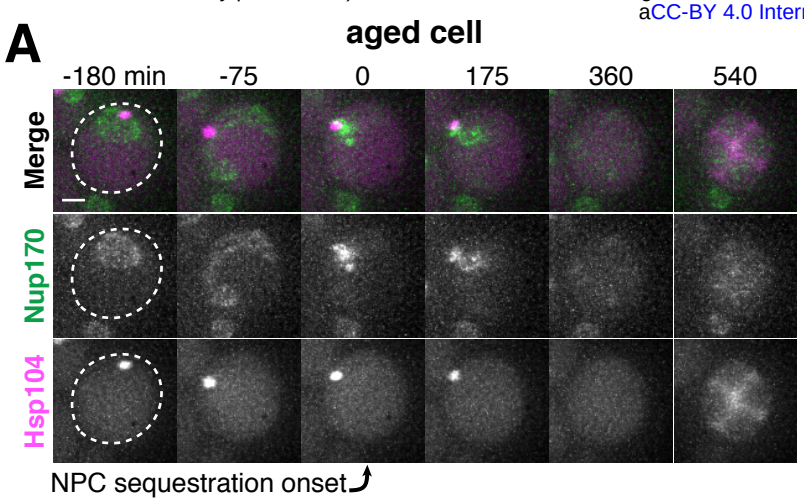

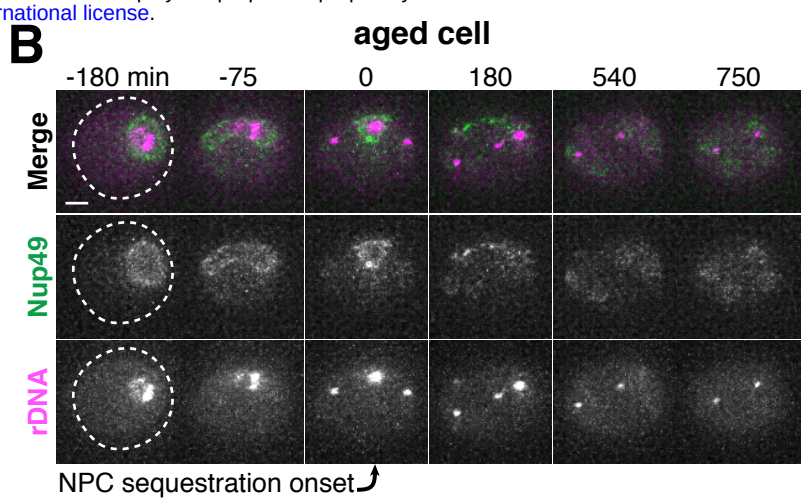

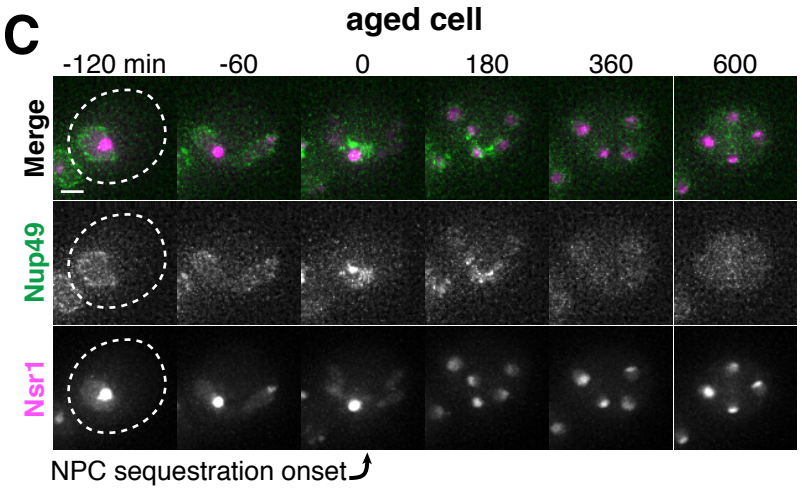

King and Goodman et al. Figure 4

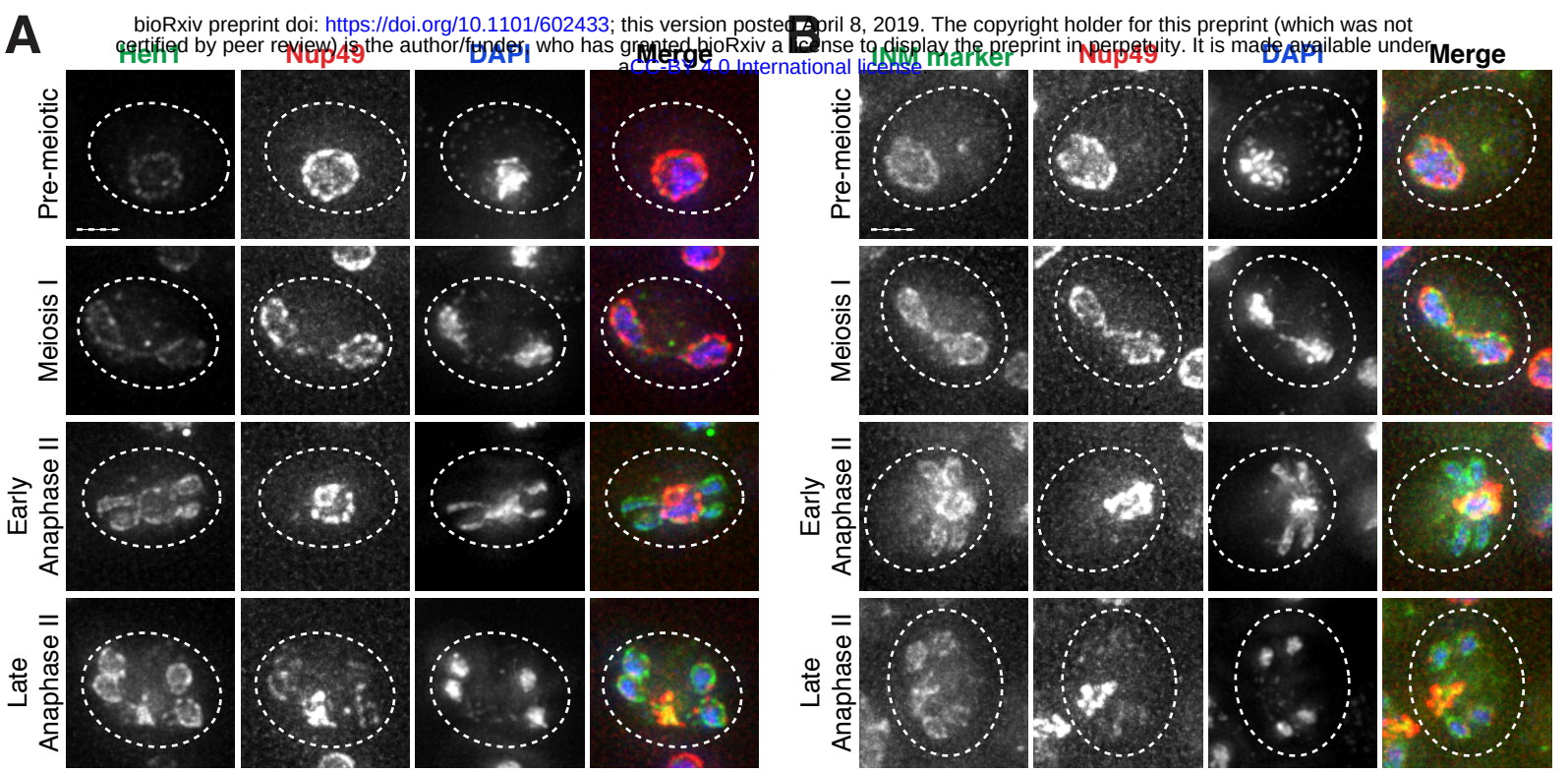

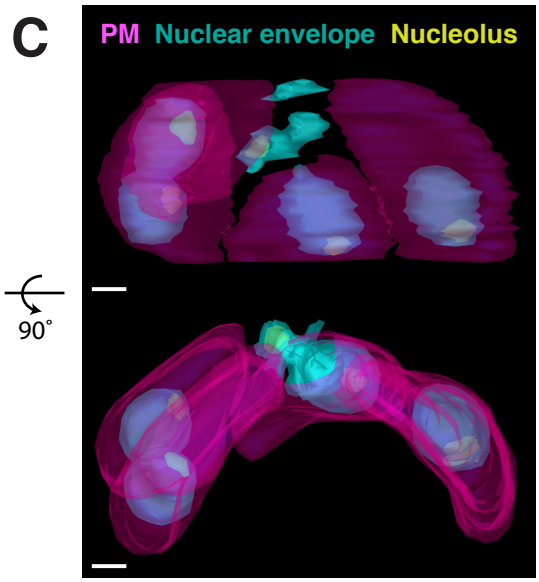

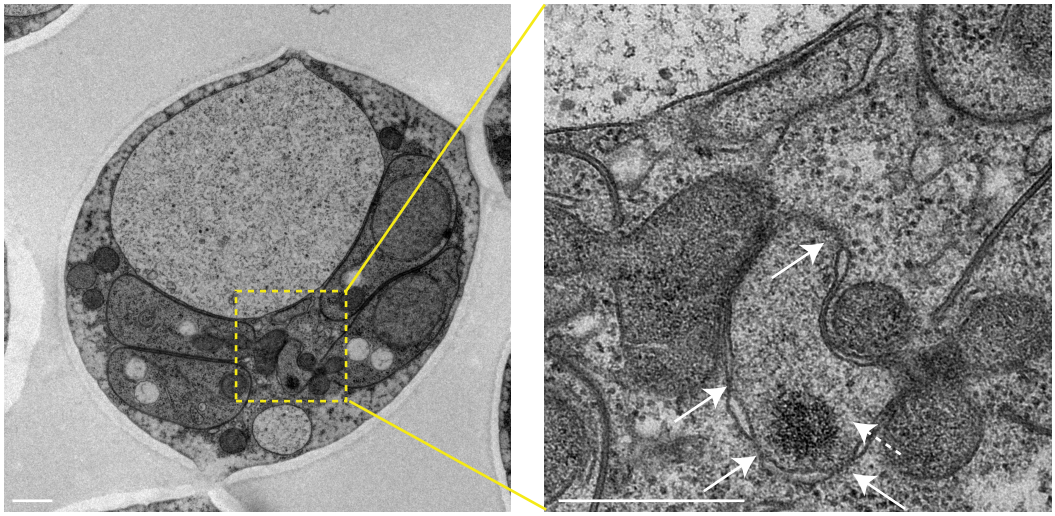

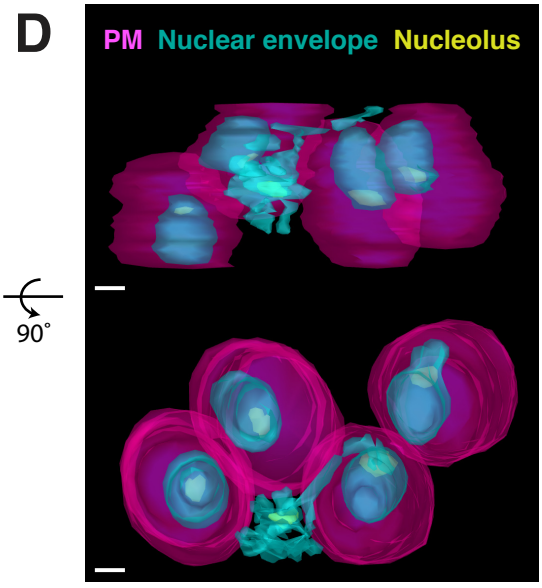

King and Goodman et al. Figure 5

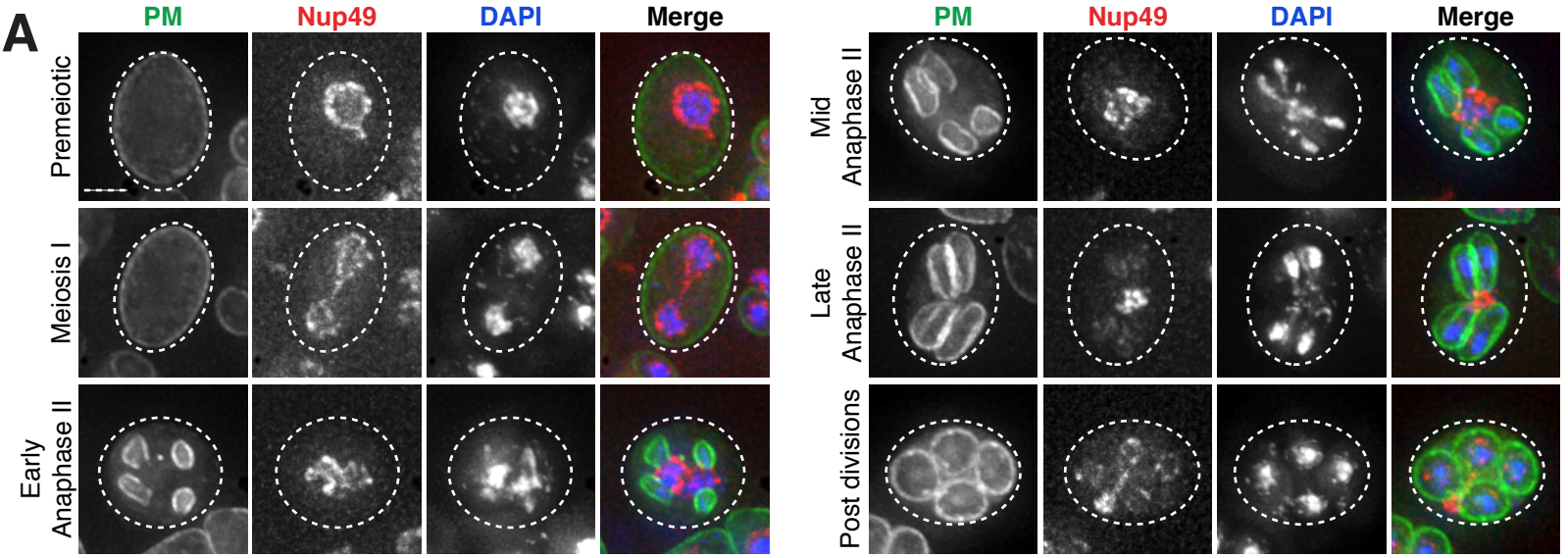

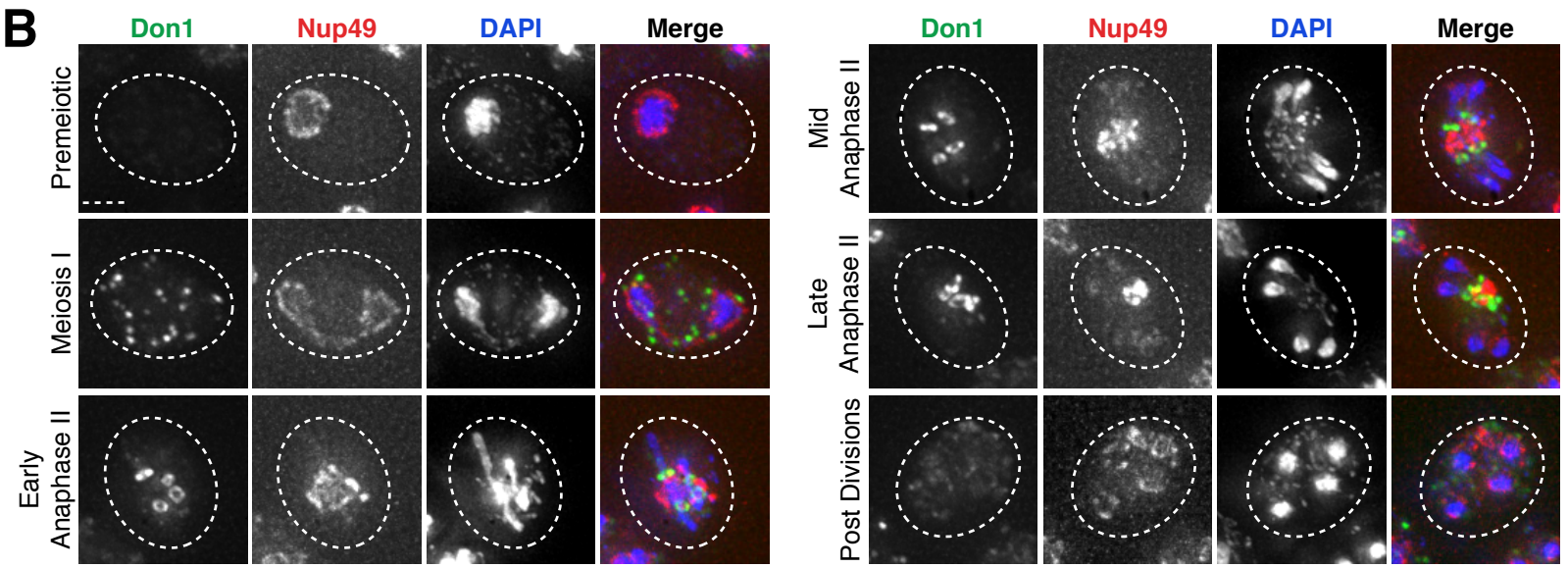

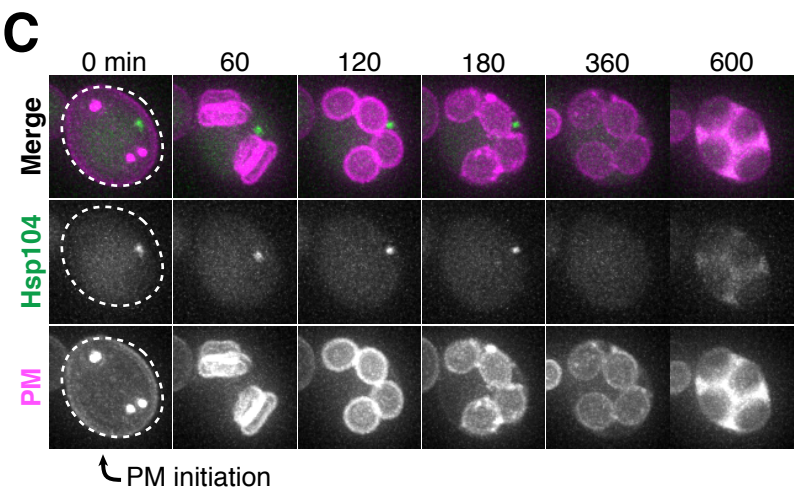

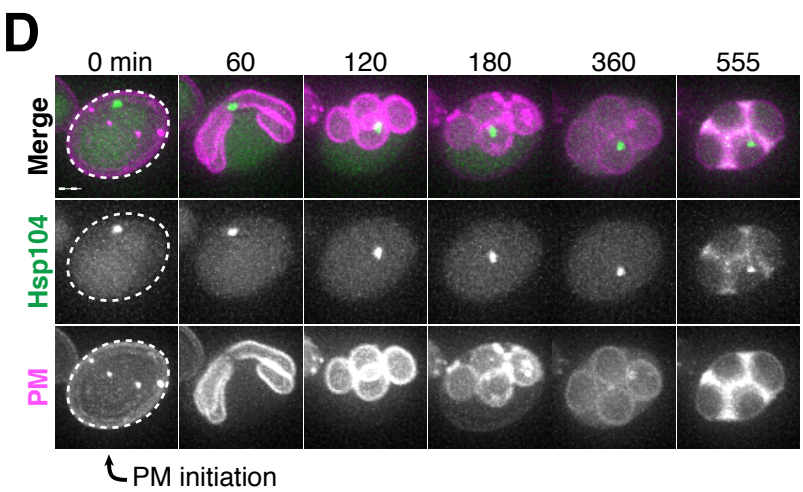

King and Goodman et al. Figure 6

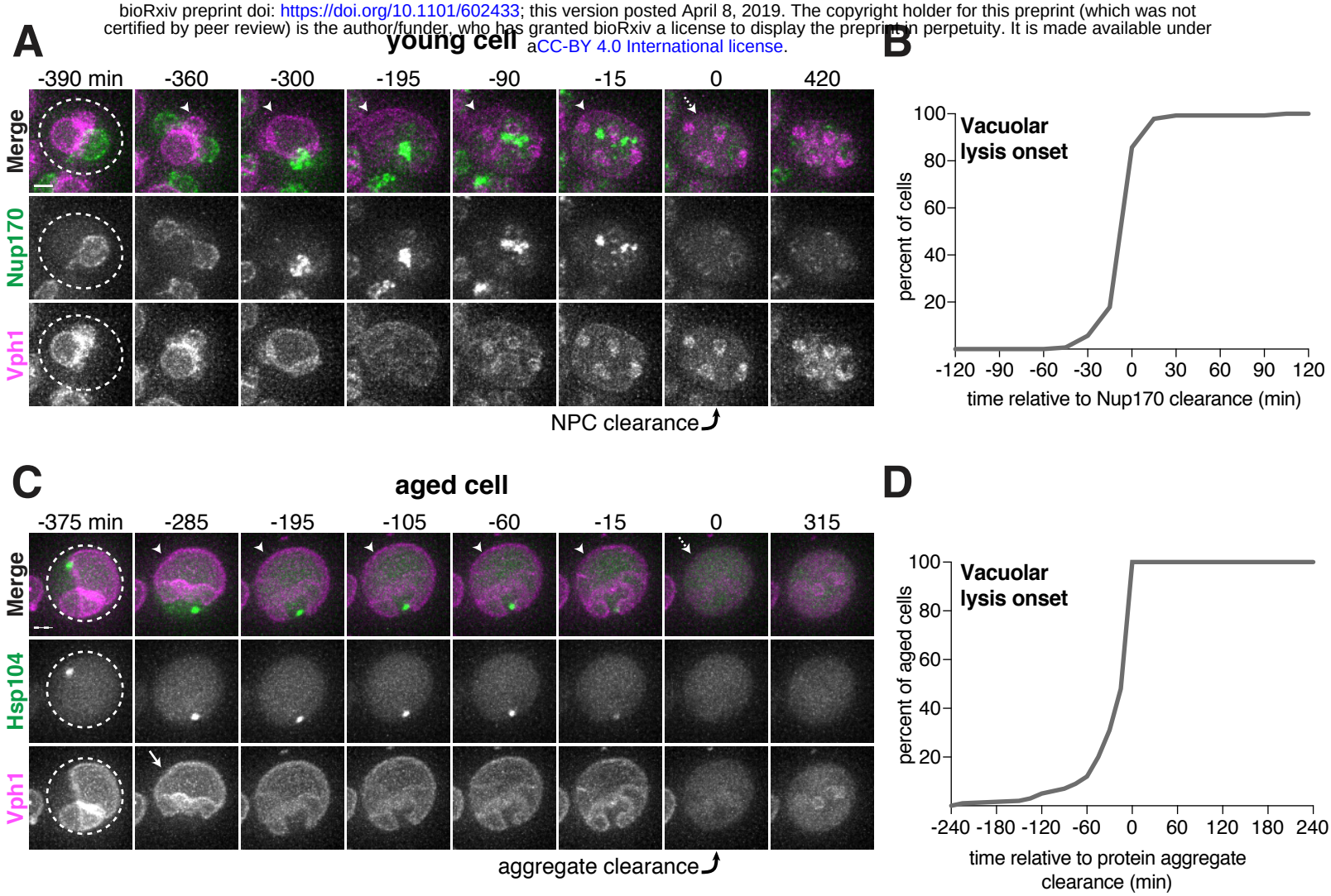

King and Goodman et al. Figure 7

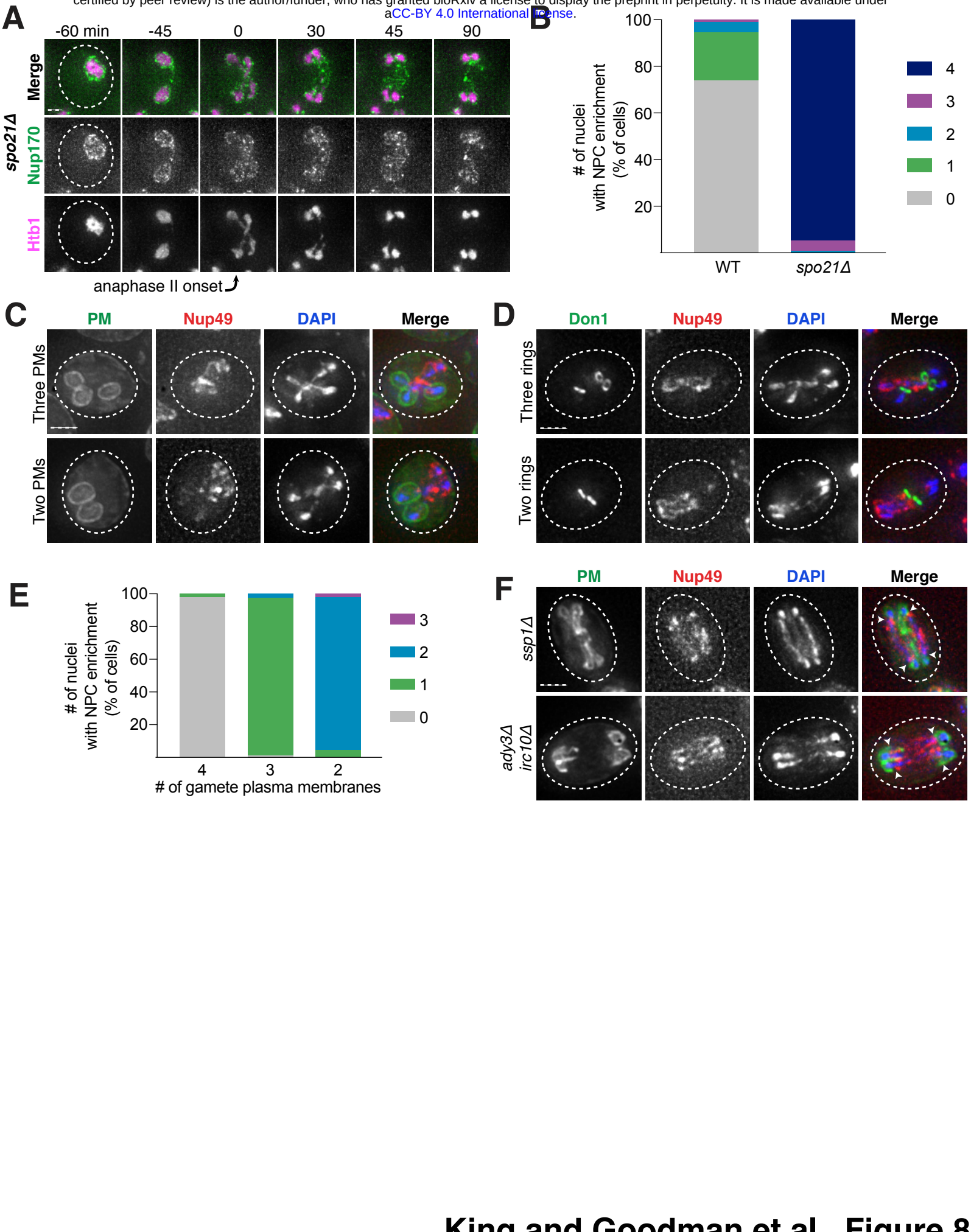

King and Goodman et al. Figure 8

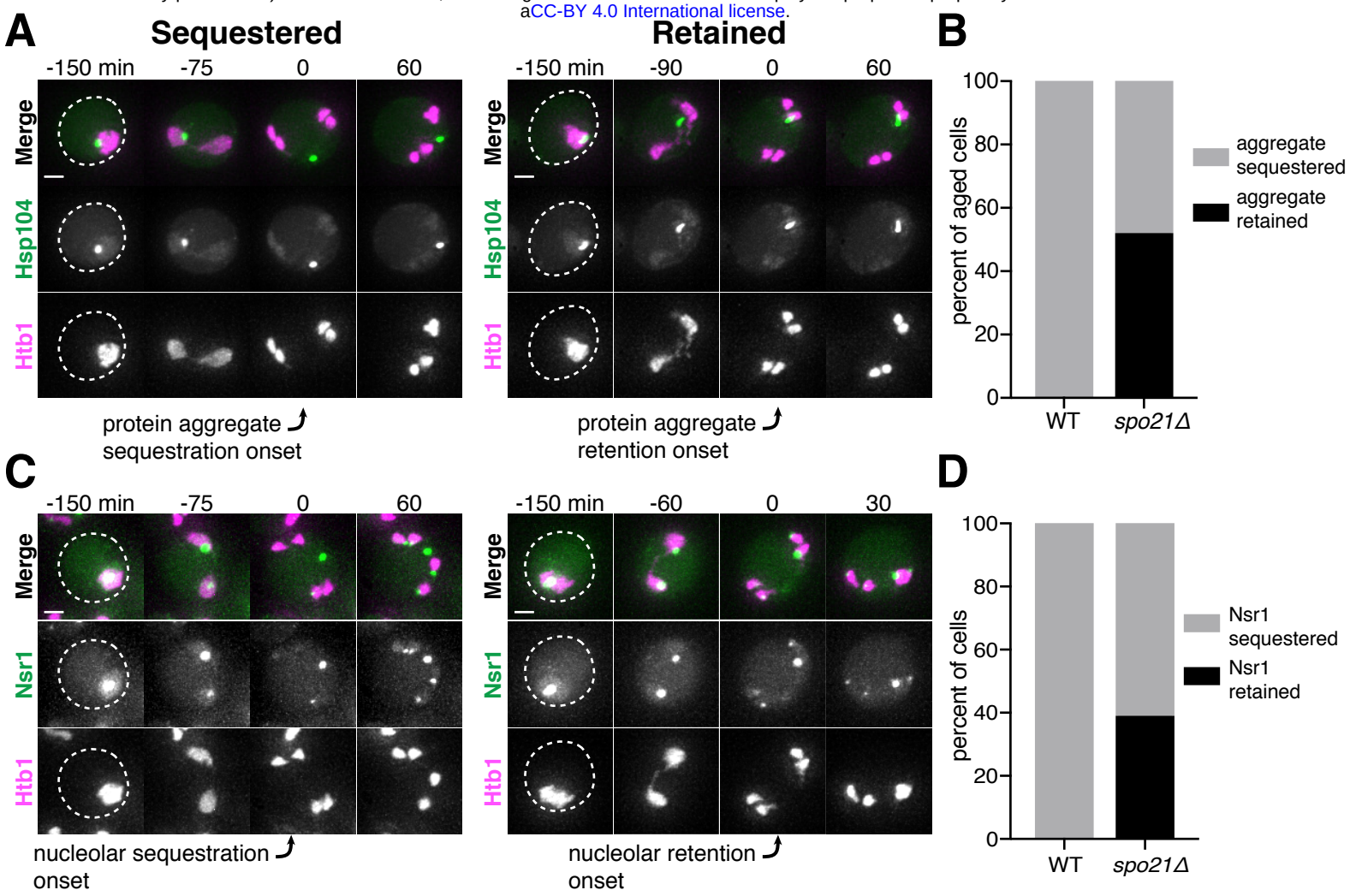

King and Goodman et al. Figure 9

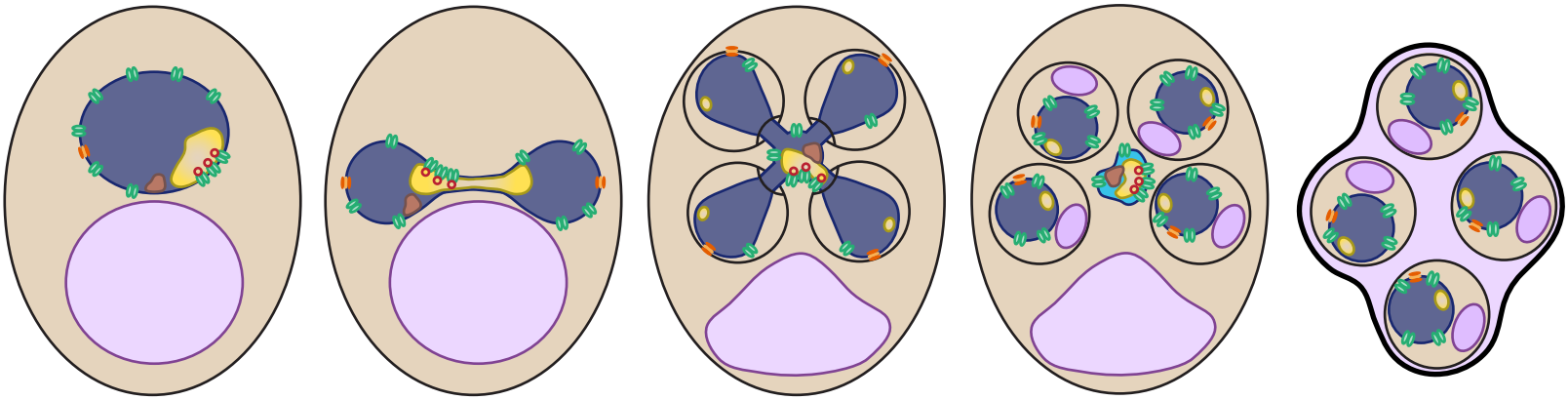

King and Goodman et al. Figure 10

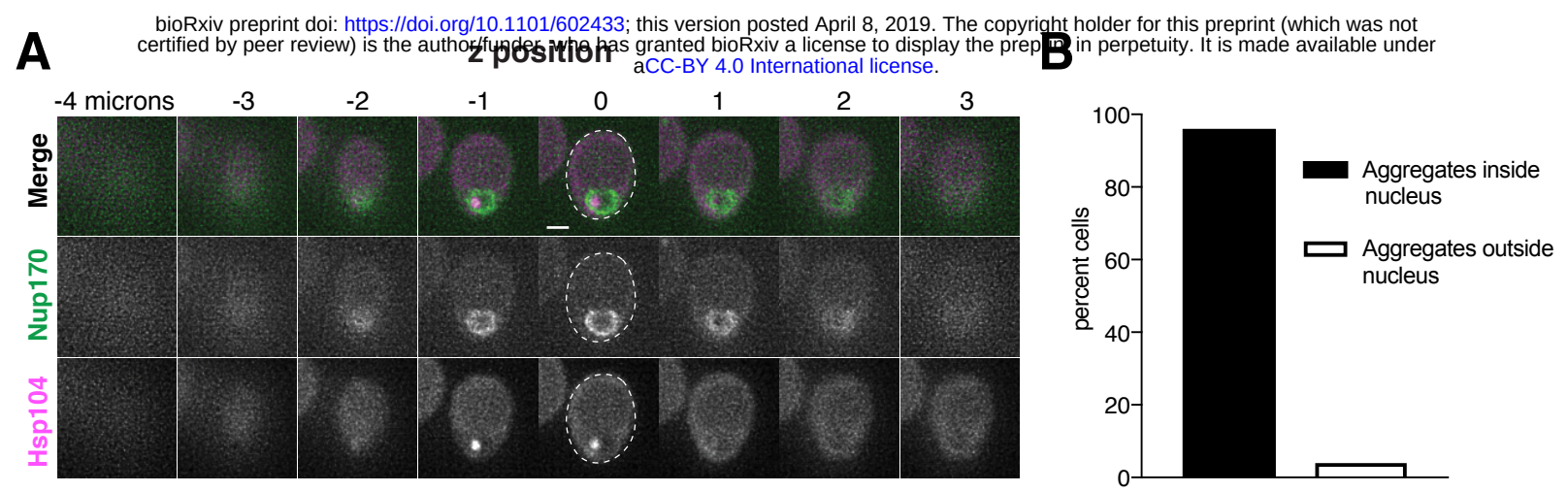

King and Goodman et al. Figure 1 - Supplement 1

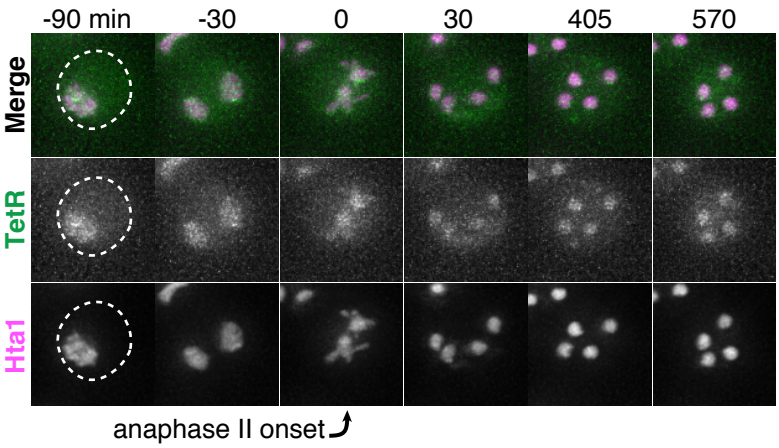

King and Goodman et al. Figure 1 - Supplement 2

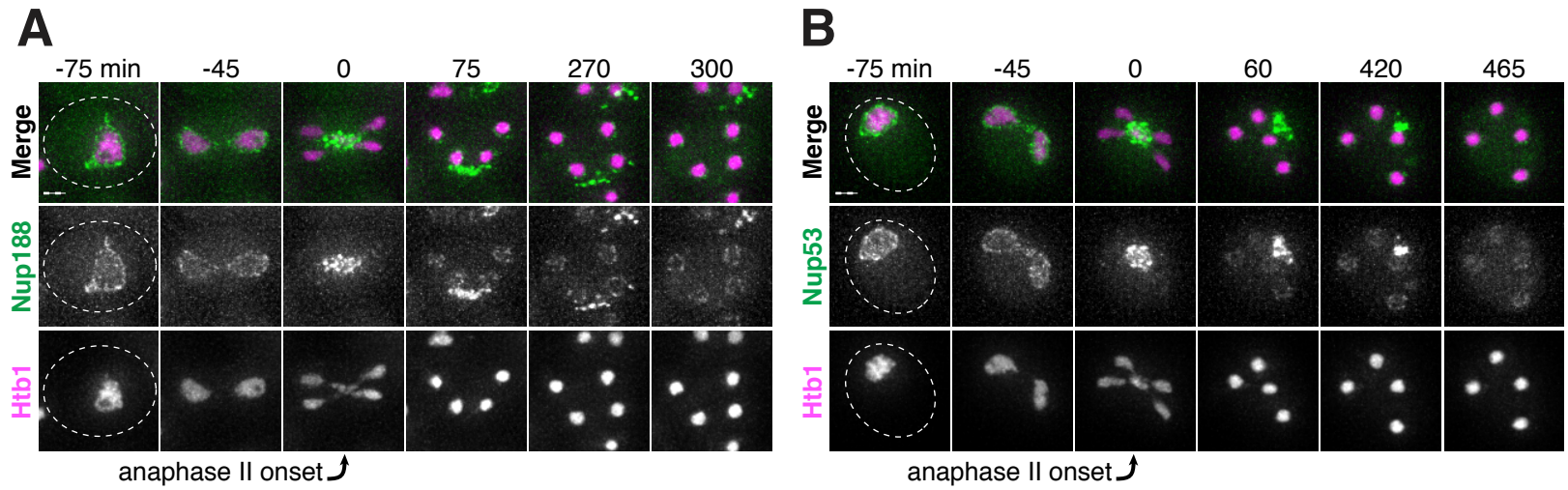

King and Goodman et al. Figure 3 - Supplement 1

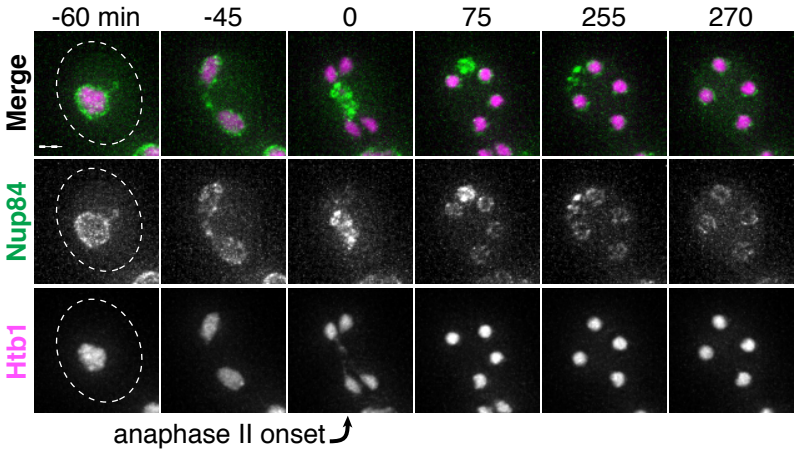

King and Goodman et al. Figure 3 - Supplement 2

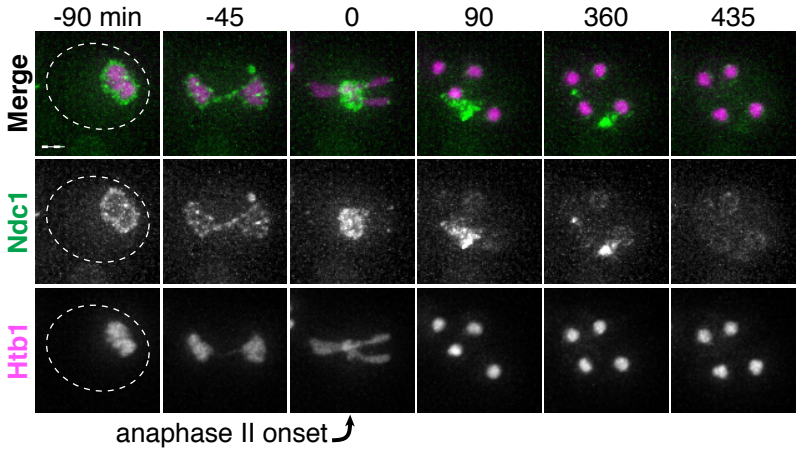

King and Goodman et al. Figure 3 - Supplement 3

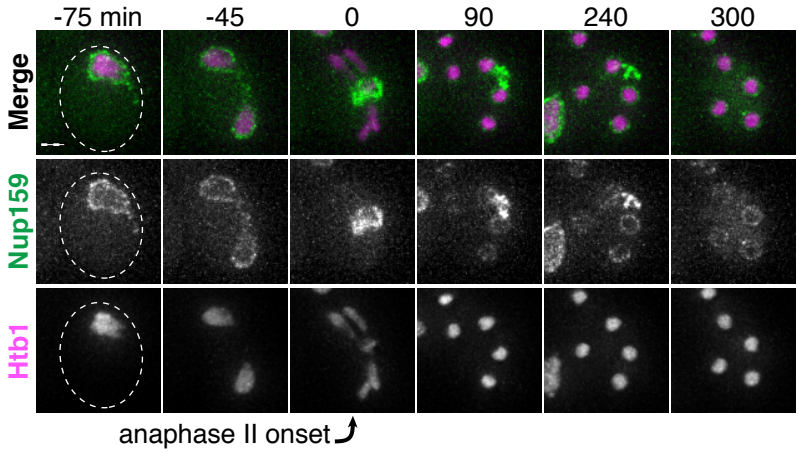

King and Goodman et al. Figure 3 - Supplement 4

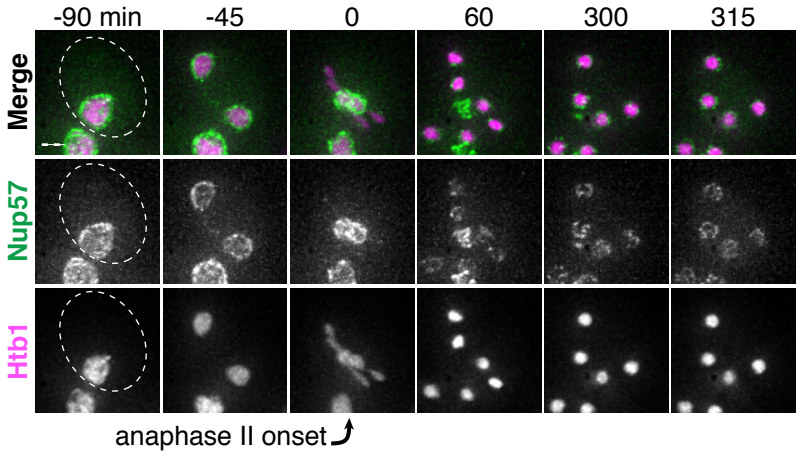

King and Goodman et al. Figure 3 - Supplement 5

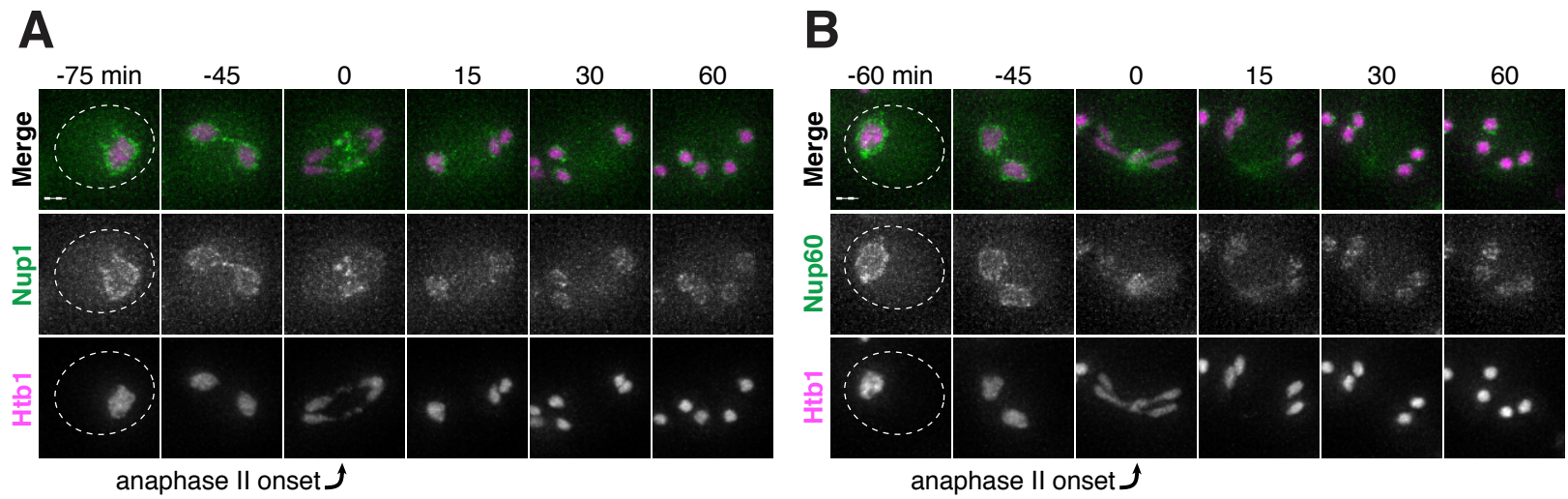

King and Goodman et al. Figure 3 - Supplement 6

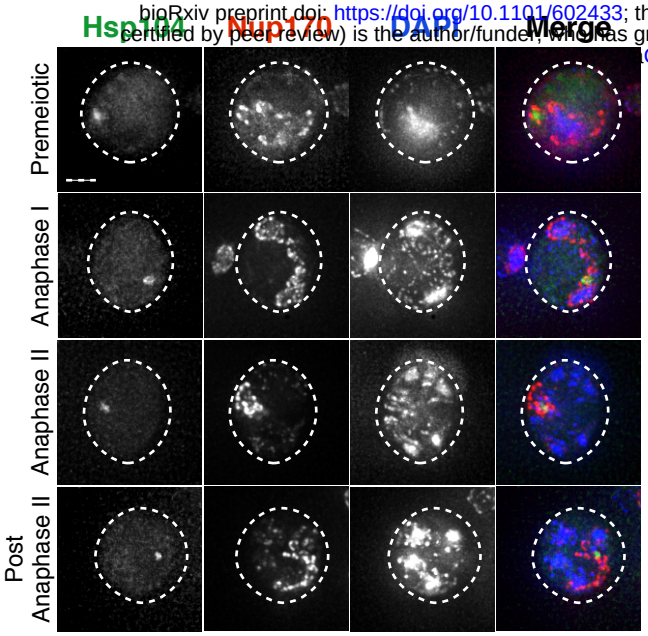

King and Goodman et al. Figure 4 - Supplement 1

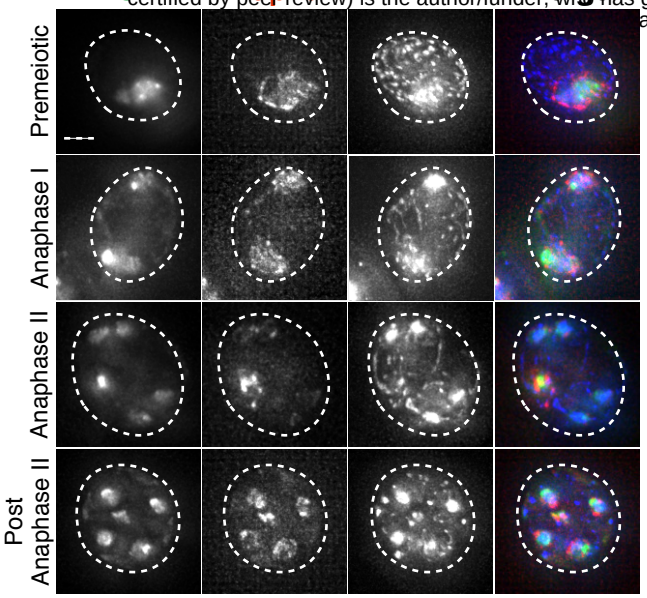

King and Goodman et al. Figure 4 - Supplement 2

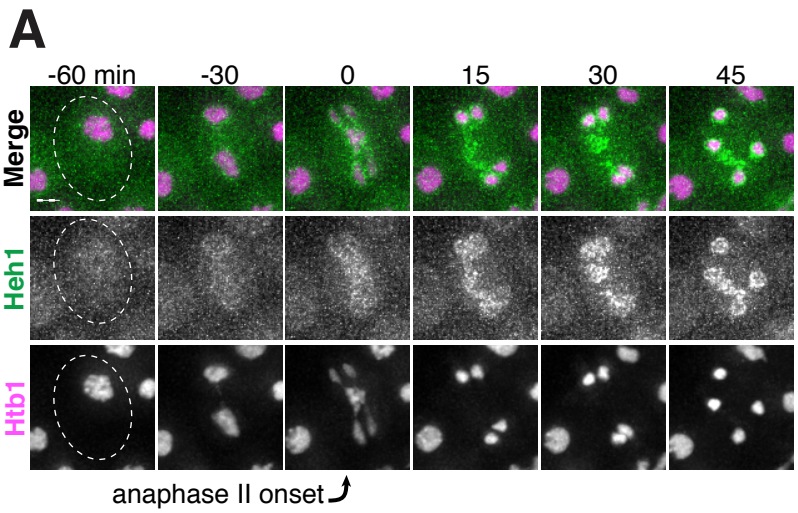

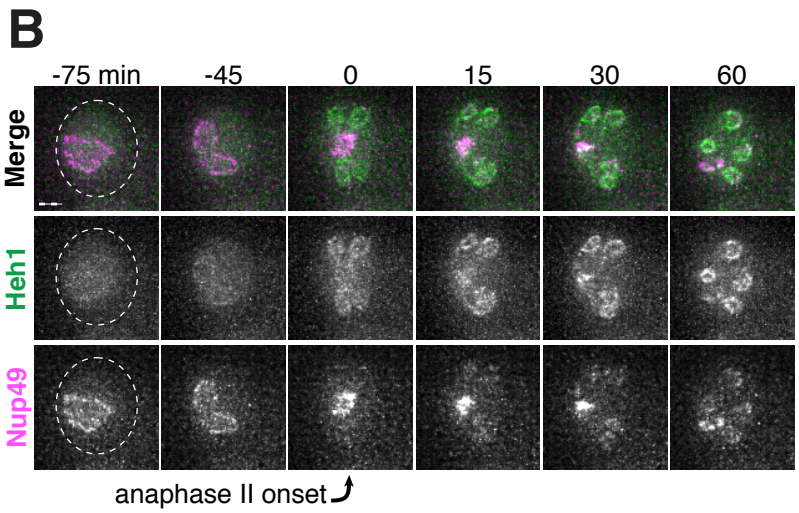

King and Goodman et al. Figure 5 - Supplement 1

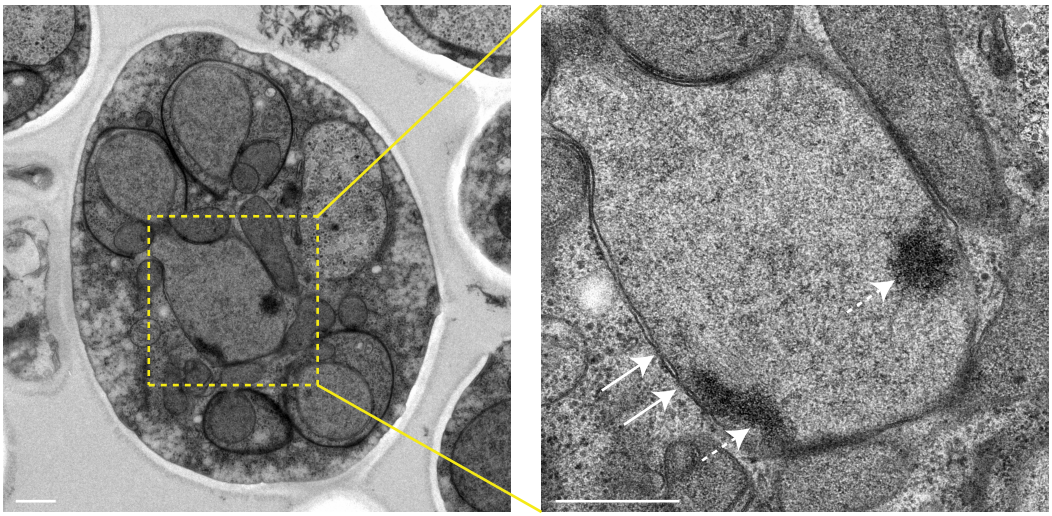

King and Goodman et al. Figure 5 - Supplement 2

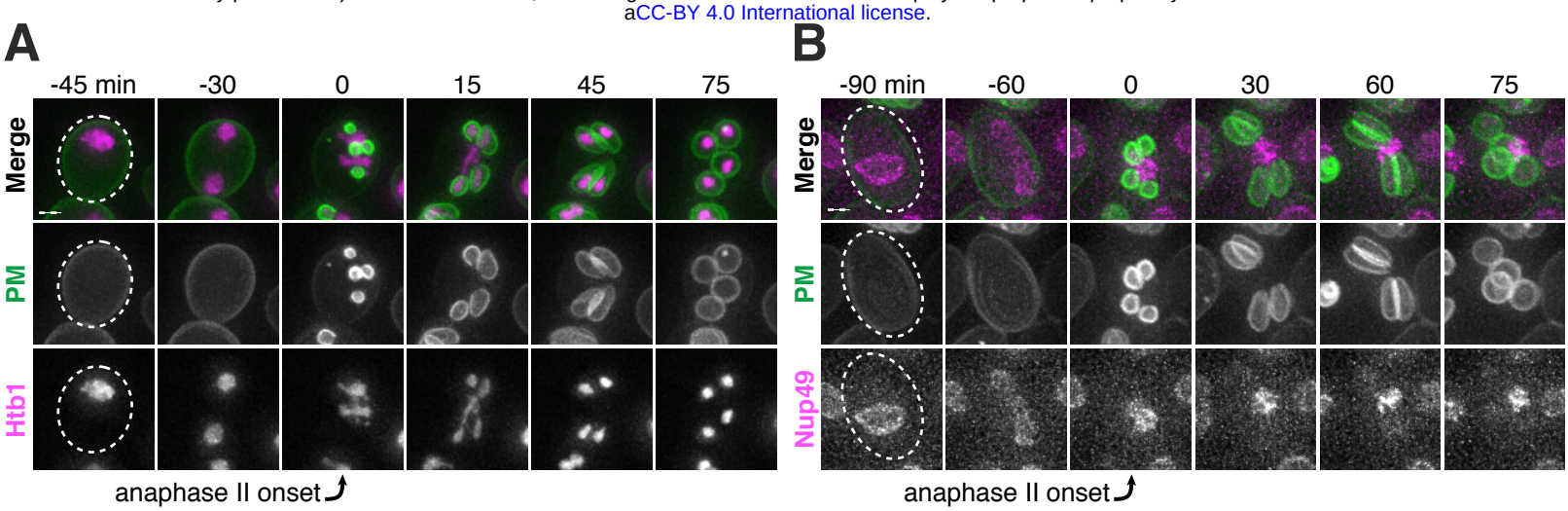

King and Goodman et al. Figure 6 - Supplement 1

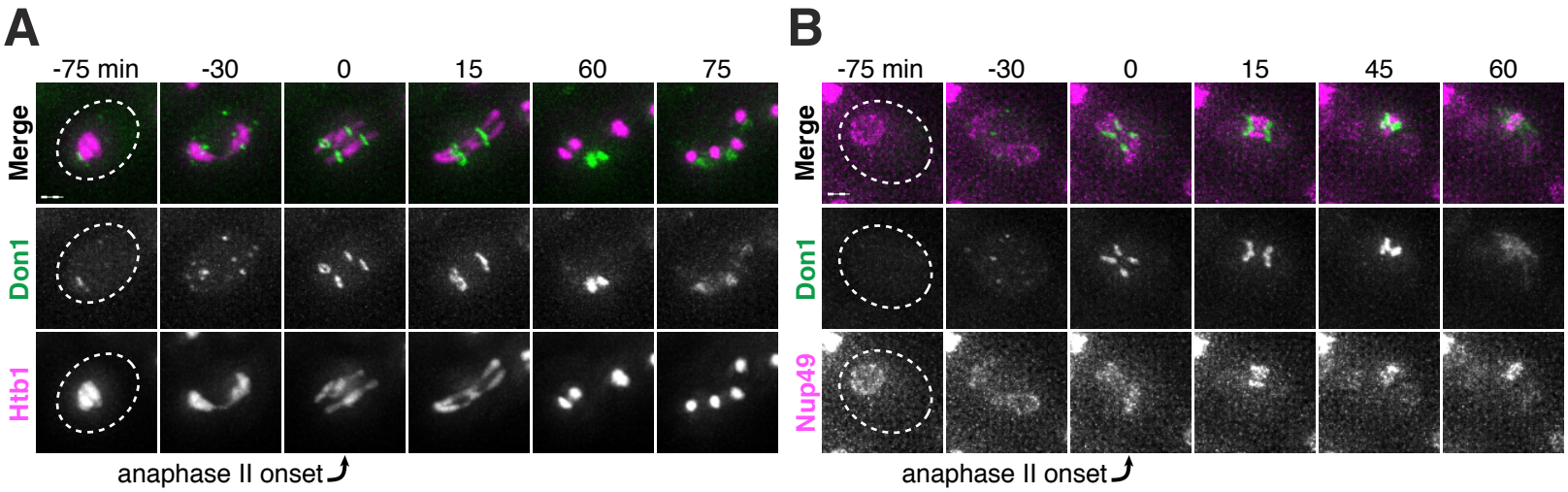

King and Goodman et al. Figure 6 - Supplement 2

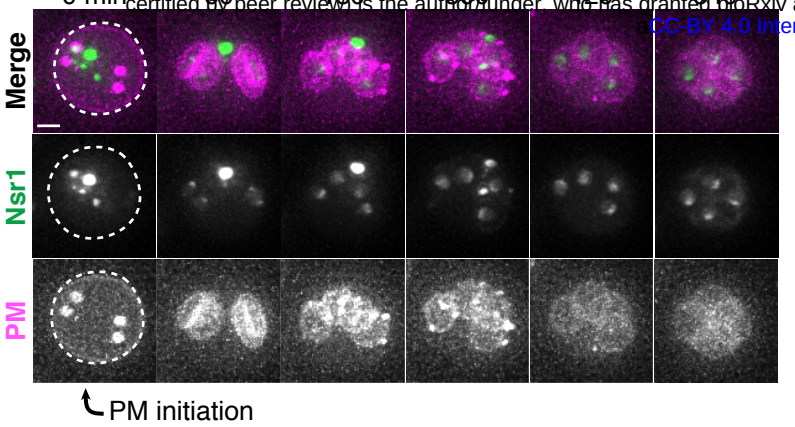

King and Goodman et al. Figure 6 - Supplement 3

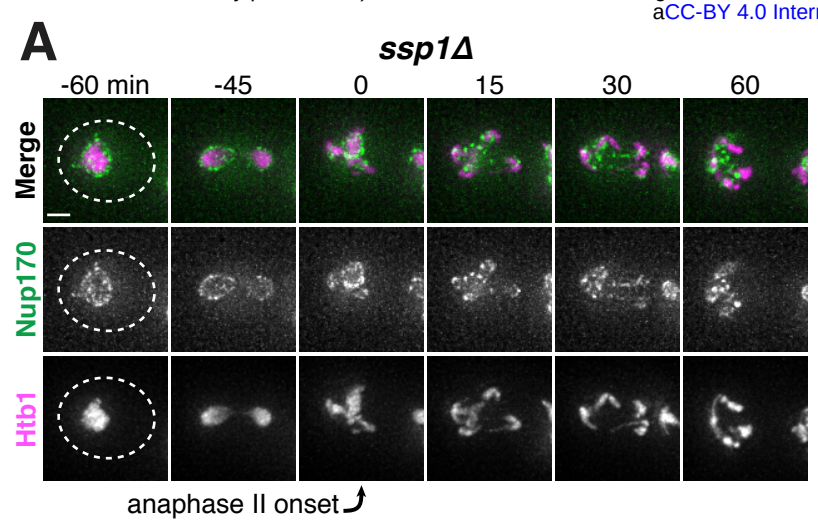

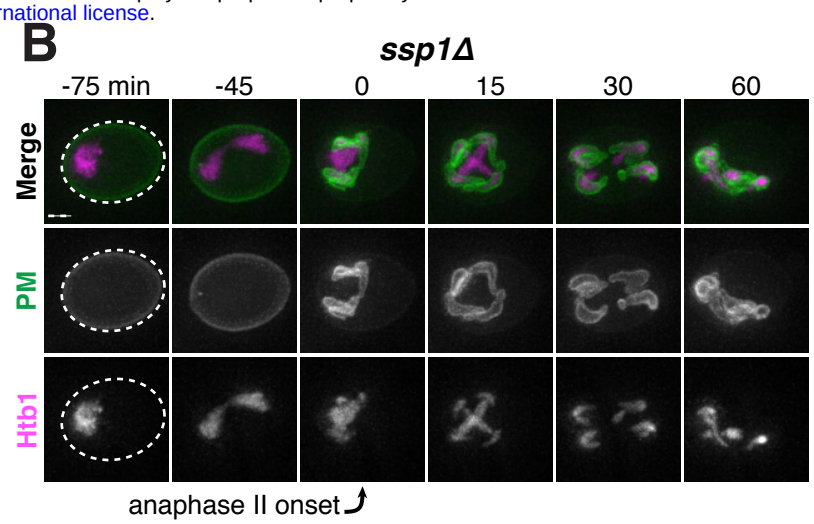

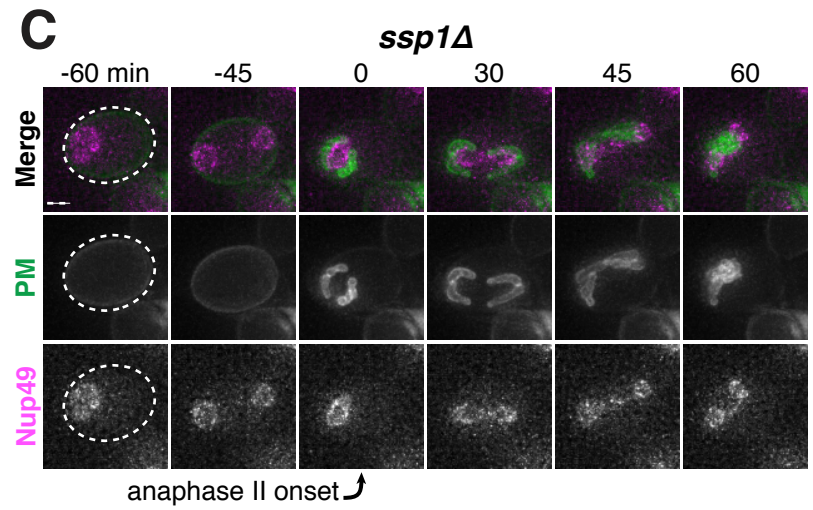

King and Goodman et al. Figure 8 - Supplement 1

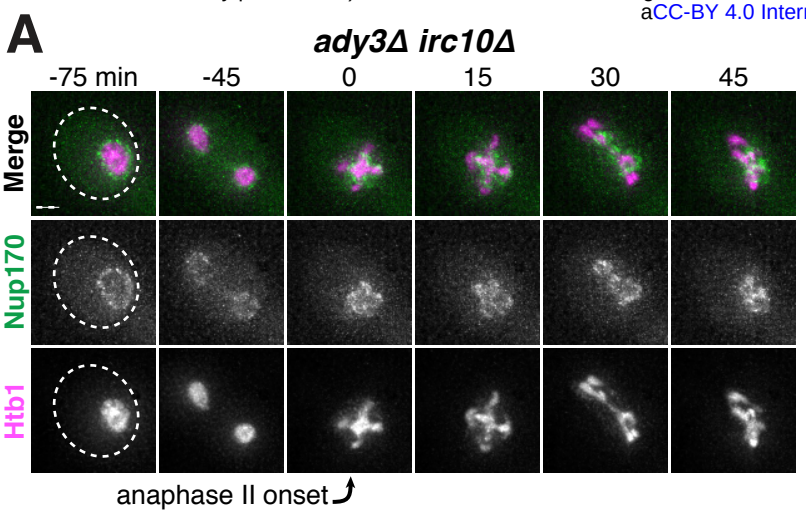

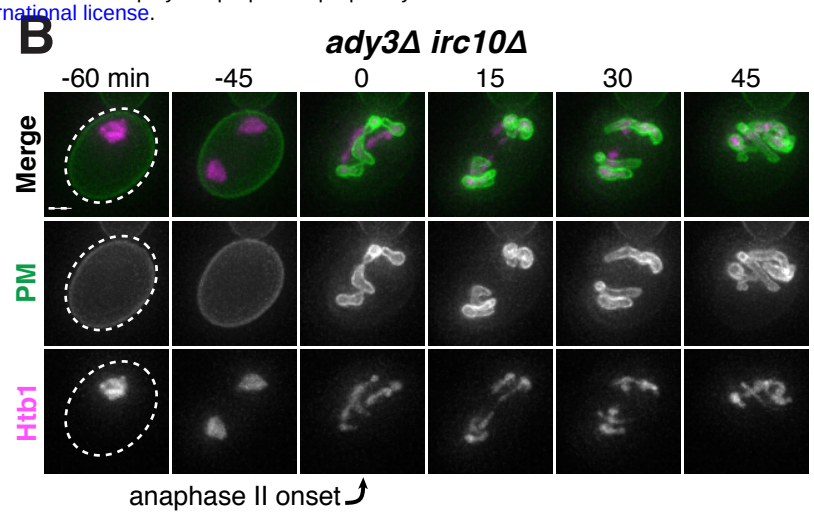

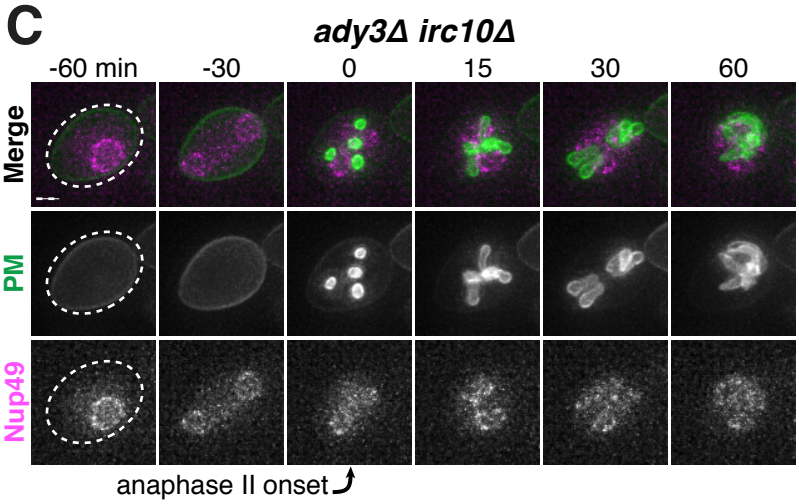

King and Goodman et al. Figure 8 - Supplement 2

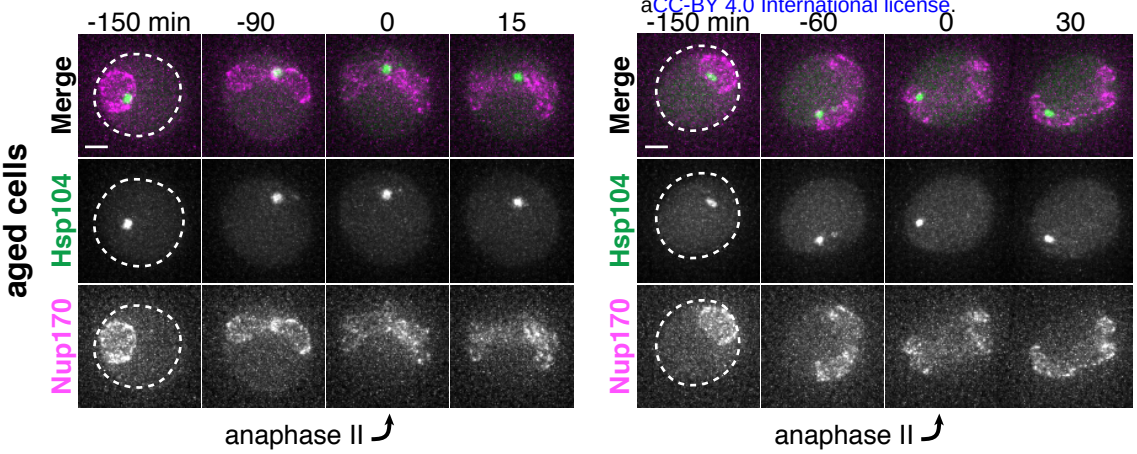

King and Goodman et al. Figure 9 - Supplement 1

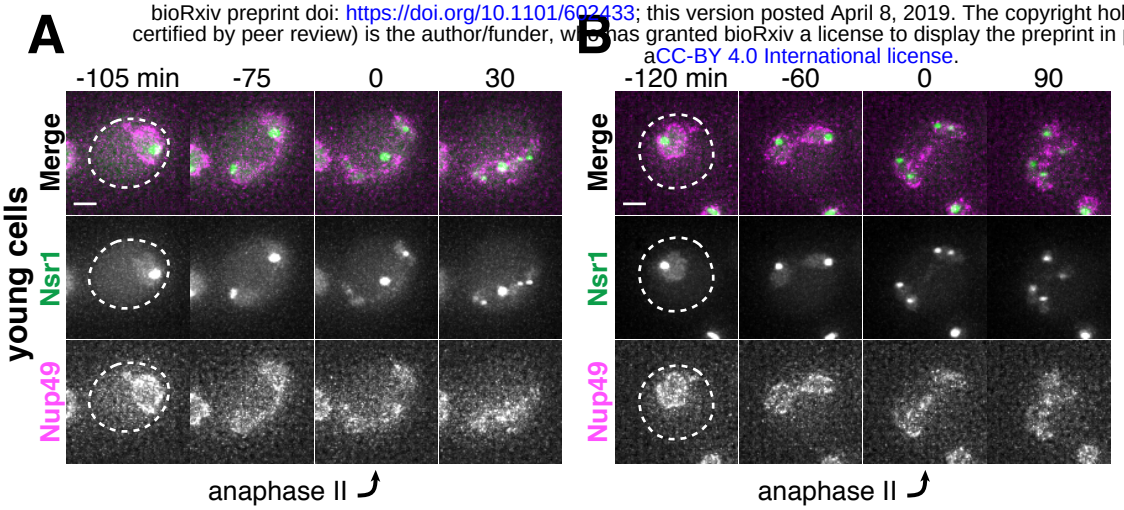

King and Goodman et al. Figure 9 Supplement 2